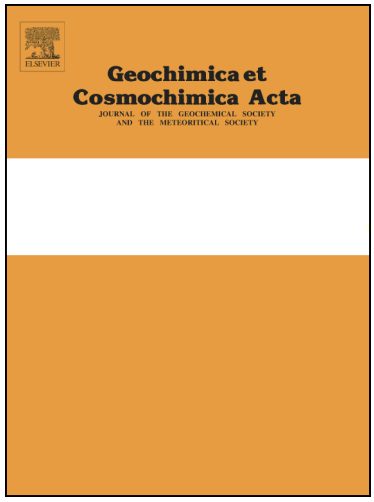

$^{40}Ar/^{39}Ar$ impact ages and time-temperature argon diffusion history of the Bunburra Rockhole anomalous basaltic achondrite

F. Jourdan, G. Benedix, E. Eroglu, P.A. Bland, A. Bouvier

PII: S0016-7037(14)00386-X
DOI: http://dx.doi.org/10.1016/j.gca.2014.05.039
Reference: GCA 8841

To appear in: *Geochimica et Cosmochimica Acta*

Received Date: 6 August 2013
Accepted Date: 26 May 2014

Please cite this article as: Jourdan, F., Benedix, G., Eroglu, E., Bland, P.A., Bouvier, A., $^{40}Ar/^{39}Ar$ impact ages and time-temperature argon diffusion history of the Bunburra Rockhole anomalous basaltic achondrite, *Geochimica et Cosmochimica Acta* (2014), doi: http://dx.doi.org/10.1016/j.gca.2014.05.039

$^{40}Ar/^{39}Ar$ impact ages and time-temperature argon diffusion history of the Bunburra Rockhole anomalous basaltic achondrite

F. Jourdan[1*], G. Benedix[2], E. Eroglu[3], P.A. Bland[2], A. Bouvier[4]

[1]*Western Australian Argon Isotope Facility, Department of Applied Geology and JdL-CMS, Curtin University, GPO Box U1987, Perth, WA 6845, Australia.*

[2]*Department of Applied Geology, Curtin University, GPO Box U1987, Perth, WA 6845,*

[3]*School of Chemistry and Biochemistry, The University of Western Australia, Crawley, WA 6009, Australia.*

[4]*Department of Earth Sciences, University of Western Ontario, London, ON, N6A 3K7, Canada*

**corresponding author*

Abstract

The Bunburra Rockhole meteorite is a brecciated anomalous basaltic achondrite containing coarse-, medium- and fine-grained lithologies. Petrographic observations constrain the limited shock pressure to between ca. 10 GPa and 20 GPa. In this study, we carried out nine $^{40}Ar/^{39}Ar$ step-heating experiments on distinct single-grain fragments extracted from the coarse and fine lithologies. We obtained six plateau ages and three mini-plateau ages. These ages fall into two internally concordant populations with mean ages of 3640 ± 21 Ma (n=7; P=0.53) and 3544 ± 26 Ma (n=2; P=0.54),

respectively. Based on these results, additional $^{40}Ar/^{39}Ar$ data of fusion crust fragments, argon diffusion modeling, and petrographic observations, we conclude that the principal components of the Bunburra Rockhole basaltic achondrite are from a melt rock formed at ~3.64 Ga by a medium to large impact event. The data imply this impact generated high enough energy to completely melt the basaltic target rock and reset the Ar systematics, but only partially reset the Pb-Pb age. We also conclude that a complete $^{40}Ar^*$ resetting of pyroxene and plagioclase at this time could not have been achieved at solid-state conditions. Comparison with a terrestrial analogue (Lonar crater) shows that the time-temperature conditions required to melt basaltic target rocks upon impact are relatively easy to achieve. Ar data also suggest that a second medium-size impact event occurred on a neighboring part of the same target rock at ~3.54 Ga. Concordant low-temperature step ages of the nine aliquots suggest that, at ~3.42 Ga, a third smaller impact excavated parts of the ~3.64 Ga and ~3.54 Ga melt rocks and brought the fragments together. The lack of significant impact activity after 3.5 Ga, as recorded by the Bunburra Rockhole suggest that (1) either the meteorite was ejected in a small secondary parent body where it resided untouched by large impacts, or (2) it was covered by a porous heat-absorbing regolith blanket which, when combined with the diminishing frequency of large impacts in the solar system, protected Bunburra from subsequent major heating events. Finally we note that the total (K/Ar) resetting impact event history recorded by some of the brecciated eucrites (peak at 3.8-3.5 Ga) is similar to the large impact history recorded by the Bunburra Rockhole parent body (ca. 3.64-3.54 Ga; this study) and could indicate a similar position in the asteroid belt at that time.

Keywords: anomalous basaltic achondrite, impact event, $^{40}Ar/^{39}Ar$ thermochronology

Introduction

Basaltic achondrites are mafic and ultramafic igneous rocks produced by magmatic differentiation at the surface, or within the crust, of relatively large parent bodies (McSween et al., 2011). These bodies likely had a metallic core, overlain by a silicate mantle and crust (e.g., Greenwood et al., 2005; Weiss and Elkins-Tanton, 2013). Eucrites are the most dominant type of basaltic achondrites, although the latter group also comprises meteorite types such as ultramafic angrites (e.g., Mittlefehldt et al., 1998). The basaltic achondrites have similar mineralogy to terrestrial basalts, and are mostly composed of plagioclase and pyroxene, but can also include olivine and accessory phases such as micro-zircon. A common oxygen isotopic signature for the majority of the Eucrites, as well as the Howardites and Diogenites (together forming the HED group) meteorites suggests that they originate from a common asteroid parent body (Clayton and Mayeda, 1996; Greenwood et al., 2005). Based on visible and near infrared reflectance spectroscopy, the principal parent asteroid of HED meteorites is generally thought to be the asteroid 4 Vesta, the largest differentiated asteroid in the main belt. HEDs are likely derived from the Vestoids, a family of small asteroids orbitally related to Vesta that bridge the gap between Vesta and meteorite-delivering resonances (Burbine et al., 2001). Although the connection between HED meteorites and asteroid 4 Vesta is not universally accepted (e.g., Schiller et al., 2011), recent results from the Dawn spacecraft mission, which arrived at 4 Vesta in July 2011, have somewhat reinforced this hypothesis (Russell et al., 2012).

In addition to the ‘normal’ eucrites, a minority of anomalous basaltic achondrites (eleven specimens discovered so far, such as NWA 011 and Ibitira; Yamaguchi et al. (2002)) have major element compositions similar to other eucrites, but distinct trace element concentrations

and, most importantly $\Delta^{17}O$ values, significantly departing from the HED-type eucrite meteorites. Due to their distinct $\Delta^{17}O$ signatures, these anomalous basaltic achondrites have been proposed to: (1) belong to distinct parent bodies, similar in nature, but unrelated to 4 Vesta, (2) originate from 4 Vesta but from a region where the parent body did not undergo complete oxygen homogenisation (Scott et al., 2009; Yamaguchi et al., 2002), and (3) originate from Vesta, but prior to or during impact ejection had their oxygen composition modified by an impactor 'contaminant' or late veneers (Greenwood et al., 2013).

The Bunburra Rockhole (hereafter Bunburra) meteorite is a recently recovered anomalous basaltic achondrite for which orbital parameters have been determined: Bunburra's fall was recorded by the Desert Fireball Network in July 2007 (Bland et al., 2009), thus giving this meteorite a unique context relative to other anomalous basaltic achondrites. Here, we report new, exceptionally well-behaved, $^{40}Ar/^{39}Ar$ analyses of various fragments of the Bunburra meteorite coupled with argon diffusion models to constrain the thermal and impact history of the Bunburra achondrite.

The Bunburra Rockhole anomalous basaltic achondrite

Bunburra is a brecciated basaltic achondrite (Fig. 1) from which three pieces weighing a total of 339 g have been recovered (Bland et al., 2009; Benedix et al., 2010). All three pieces are partially to entirely enclosed by fusion crust created during atmospheric entry on 21 July 2007. The rock is composed of anorthitic plagioclase (52.5 vol%) and pyroxene (41.5 vol%), with a minor amount of pure silica glass (4.5 vol%) and traces of sulfide, ilmenite and chromite (1.5 vol%) (Benedix et al., 2010). The mineral compositions of Bunburra are indistinguishable from normal eucrites (Benedix et al., 2010). The Bunburra meteorite is well crystallized with little or no porosity (Fig. 1) as expected for basaltic meteorites.

Bunburra contains three distinct lithologies: fine-, medium-, and coarse-grained (Fig. 1; Benedix et al., 2010; Bland et al., 2009) with similar modal composition. None of the three fractions of the Bunburra meteorite show significant evidence of intense shock pressures. The contacts between the various lithologies (i.e., coarse- against fine-grained) show some hints of plastic deformation, but no detectable evidence of melting. In thin section, observed shock features are abundant cracks, undulatory features in pyroxene and localized cloudiness in both plagioclase and pyroxene crystals (Fig. 1). These observations suggest a recorded shock pressure higher than ~10 GPa (Langenhorst and Deutsch, 2012). On the other hand, no melt pockets or veins have been observed, all feldspar grains are plagioclase without any evidence for maskelynite, diaplectic glass or planar deformation features (PDFs), suggesting shock pressure lower than ~20 GPa (Langenhorst and Deutsch, 2012; Gillet and El Goresy, 2013). The shock pressures experienced by Bunburra are thus constrained to ca. 10-20 GPa. Such a range of shock pressure corresponds to an equivalent temperature of ~250°C on the Hugoniot curve (a theoretical P-T curve which constrains the temperature value for any given pressure; Langenhorst and Deutsch, 2012) of basalt (Gillet and El Goresy, 2013). Thus, the meteorite could be classified as shock stage S3.

The $\Delta^{17}O$ compositions of the three fractions are statistically indistinguishable, with an average value of -0.13 ± 0.04 ‰ (Bland et al., 2009). The oxygen isotopic composition of Bunburra is thus distinct from the HED fractionation line with $\Delta^{17}O$ =0.24 ± 0.02 ‰. On the other hand, Bunburra lies within the oxygen isotopic range observed for Asuka-881394, Ibitira and the angrite group between ca. -0.13 and -0.06 ‰ (Clayton and Mayeda, 1996; Greenwood et al., 2005). On this basis, the Bunburra meteorite is classified as an anomalous basaltic achondrite. A distinct $\Delta^{17}O$ value suggests that the Bunburra achondrite either belongs to a unique parent body not previously sampled before, or originated from an isotopically unequilibrated part of 4 Vesta. Yamaguchi et al. (2002) and others (e.g., Scott et

al., 2009), suggested that the latter hypothesis is less likely as the complete melting and differentiation of the parent body should have resulted in complete oxygen homogenisation. Alternatively, we can envisage that the impactor signatures might have been mixed with the target rock from asteroid Vesta upon impact melting, which yielded an intermediate oxygen composition in the newly crystallized melt rock, but on the other hand, this process would have possibly given rise to different mineralogy and/or element signature compared to other HED meteorites, which is not observed. In any case, as outlined by Duffard (2009), the presence of a large number of ungrouped iron meteorites and newly discovered non-Vestoid basaltic asteroids imply that many differentiated parent bodies may have existed during the early history of the solar system.

Recent chronology studies indicate that the ^{26}Al-^{26}Mg system was fully reset while the Pb-Pb system was strongly disturbed at the mineral and whole-rock scale (Spivak-Birndorf et al., 2010). The mineral fractions (pyroxene and plagioclase) gave an errorchron age of ~4.2 Ga (MSWD = 264). However, if only the four whole-rock samples were considered, these together yielded a Pb-Pb whole-rock age of 4102 ± 24 Ma (MSWD=1.2). The Al-Mg study by Spivak-Birndorf et al. (2010) proposed that the Pb-Pb age represented a re-equilibration age after an impact heating resetting event. In addition, Welten et al. (2012) reported $^{38}Ar_c$ (^{38}Ar cosmogenic) and $^{21}Ne_c$ cosmic ray exposure (CRE) ages around 21 Ma.

To shed new light on the thermal history and chronology of this meteorite, we investigated the ^{40}Ar/^{39}Ar systematics of Bunburra Rockhole and present the results of nine fractions of two of the lithologies.

Analytical methods

Sample selection and analytical conditions

We selected a small fragment (~0.3 cm^3) of the Bunburra Rockhole meteorite. Mineral separates are usually preferred for successful analyses with the $^{40}Ar/^{39}Ar$ technique (Jourdan, 2012), but these minerals were too small to be isolated from each other and we therefore decided to analyze whole rock chips. We picked individual fragments of ca. 250 μm in diameter and separated two distinct types of groundmass: grains with coarse to medium grain size, or fine-grained texture. We chose the fragments with the best homogeneity. We also isolated chips of fusion crust for analysis to test if melting during the atmospheric entry would fully reset the K/Ar system.

Samples were loaded into three large wells within an aluminum disc measuring 1.9 cm diameter and 0.3 cm depth. These wells were bracketed by small wells that included Hb3gr hornblende used as a neutron fluence monitor for which an age of 1081.0 ± 1.1 Ma (1σ) was calculated (Renne et al., 2011) and a good in-between-grains reproducibility has been demonstrated (Jourdan et al., 2006; Jourdan and Renne, 2007). The discs were Cd-shielded (to minimize undesirable nuclear interference reactions) and irradiated for 25 hours in the Hamilton McMaster University nuclear reactor (Canada) in position 5C. The mean J-values (measurements of the neutron fluence) computed from standard grains within the small pits range from 0.009248 ± 0.000036 (0.39%) to 0.009419 ± 0.000041 (0.43%) determined as the average and standard deviation of J-values of the small wells bracketing each large well containing the sample. Mass discrimination was monitored using an automated air pipette and provided mean values ranging from 1.004850 (±0.27%) to 1.005507 (±0.32%) per dalton (atomic mass unit) relative to an air ratio of 298.56 ± 0.31 (Lee et al., 2006). The correction factors for interfering isotopes were $(^{39}Ar/^{37}Ar)_{Ca}$ = $7.30x10^{-4}$ (± 11%), $(^{36}Ar/^{37}Ar)_{Ca}$ = $2.82x10^{-4}$ (± 1%) and $(^{40}Ar/^{39}Ar)_K = 6.76x10^{-4}$ (± 32%).

The $^{40}Ar/^{39}Ar$ analyses were performed at the Western Australian Argon Isotope Facility at Curtin University. A total of 9 groundmass fragments, including five and four

singlfragments from the coarse- and fine-grained lithologies respectively, were step-heated using a 110 W Spectron Laser Systems, with a continuous Nd-YAG (IR; 1064 nm) laser rastered over the sample for one minute to ensure homogenous heating. The extracted gas was purified in a stainless steel extraction line using two SAES AP10 getters and one GP50 getter. Ar isotopes were measured in static mode using a MAP 215-50 mass spectrometer (resolution of ~450; sensitivity of $4x10^{-14}$ mol/V) with a Balzers SEV 217 electron multiplier using 9 to 10 cycles of peak-hopping. The data acquisition was performed with the Argus program written by M.O. McWilliams and run under a LabView environment. The raw data were processed using the ArArCALC software (Koppers, 2002), ages were calculated using the decay constants recommended by Renne et al. (2011) and uncertainties on the ages were calculated using the optimization model of Renne et al. (2010) based on Monte Carlo simulation and include all sources of errors.

Blanks were monitored every 3 to 4 steps and typical ^{40}Ar blanks range from 1 x 10^{-16} to 2 x 10^{-16} mol. Ar isotopic data corrected for blank, mass discrimination and radioactive decay are given in Annex 1. Individual errors in Annex 1 are given at the 1σ level.

Cosmogenic isotope corrections

Before calculating ages from the Bunburra coarse and fine aliquots, $^{36}Ar_c$ produced by reaction of the basalt with cosmic rays must be subtracted from the total ^{36}Ar. We use the cosmogenic standard $^{36}Ar/^{38}Ar$ ratio (0.65; see details for example in Korochantseva et al. (2007)) resulting in the ^{36}Ar consisting entirely of trapped (initial) argon. This approach is valid only if $^{38}Ar_{Cl}$ (induced from chlorine during reactor irradiation; McDougall and Harrison, 1999)) is absent from the sample. In practice, however, the very low abundance measured for ^{38}Ar (and ^{36}Ar) for each particle of the Bunburra meteorite is very close to background compared to the large signal obtained for $^{40}Ar^*$, ^{39}Ar and ^{37}Ar. Thus, the

cosmogenic correction is negligible. Note that a cosmogenic correction was not applied to the fusion crust samples, as fusion crust was generated during atmosphere entry and was therefore assumed to be terrestrially formed.

$^{40}Ar/^{39}Ar$ age calculation

Our criteria for the determination of plateaus are as follow: plateaus must include at least 70% of the total ^{39}Ar and should be distributed over a minimum of 3 consecutive steps agreeing at 95% confidence level and satisfying a probability of fit (P) of at least 0.05. Plateau ages (Table 1 and Fig. 2 and 3) are given at the 2σ level and are calculated using the mean of all the plateau steps, each weighted by the inverse variance of their individual analytical error. Mini-plateaus are defined similarly except that they include between 50% and 70% of ^{39}Ar. As such, these ages are less reliable than true plateau ages (Jourdan et al., 2009; Jourdan, 2012). No inverse isochron calculations were carried out in this study as all steps essentially plot on the x-axis (i.e., radiogenic axis) demonstrating that no trapped argon was present in the sample. Ca/K spectra (derived from $^{37}Ar/^{39}Ar$) are given in Annex 2.

The uncertainties on individual plateau ages do not include external errors (although these uncertainties are provided in Table 1), but the final weighted mean of a particular event includes all sources of uncertainties (including the decay constant uncertainties). For an easy read, an uncertainty that includes all sources of uncertainties is given within brackets as ± [xx] Ma.

Calculation of exposure ages

Cosmic ray exposure (CRE) ages were tentatively calculated based on the very little quantity of $^{38}Ar_c$ in the Bunburra meteorite. Because of the spallation of Ca to ^{38}Ar due to the interaction of cosmic rays with target atoms in the sample, an exposure age can be calculated

if the amount of ^{38}Ar within the sample per gram of Ca is known. We use the cosmochron approach proposed by Levine et al. (2007) and the detailed procedures and equations given by Kennedy et al. (2013). We present the Ar isotopic data within $^{38}Ar/^{36}Ar$ vs. $^{37}Ar/^{36}Ar$ plots. The $^{38}Ar_c/^{37}Ar$ ratios were calculated for each particle using the slope of the cosmochron and converted into the $^{38}Ar/Ca$ ratio of the sample by comparison with the Hb3gr standard that has a known K/Ca ratio. Exposure ages were calculated using a Ca production rate of 2.05 x 10^{-8} cm^3 STP /gram of Ca/Ma for eucrite (Eugster and Michel, 1995; Kennedy et al., 2013; Korochantseva et al., 2007). All uncertainties are included in the error calculations.

Results

$^{40}Ar/^{39}Ar$ results: Bunburra basaltic achondrite

We obtained six plateau ages and three mini-plateau ages (Fig. 2 and 3; Table 1) for the nine samples. The ages can be grouped into two concordant populations based on the χ^2 statistical test (Figs. 4 and 5). The oldest age group includes five plateau ages ranging from 3596 ± 57 Ma (P = 0.77) to 3647 ± 35 Ma (P = 0.65) and two mini-plateau ages of 3656 ± 53 Ma (P = 0.35) and 3658 ± 36 Ma (P = 0.68; Fig. 4). These data include three ages obtained on coarse-grained particles and four ages obtained on fine-grained particles that are statistically indistinguishable with overall MSWD and P-values (statistical tests of the concordance of a data population) of 0.85 and 0.53, respectively. Since these values are concordant, we can calculate a weighted mean age of 3640 ± 18 Ma, using internal errors only and propagate the external errors on the final value using the optimized model of Renne et al. (2010) and R-Value between FCs and Hb3gr standards of Jourdan and Renne (2007). We obtained an age of **3640 ± [21] Ma**, which includes all sources of uncertainty. The second age cluster includes one plateau and one mini-plateau age of 3538 ± 30 Ma (P = 0.83) and 3553 ± 38 Ma (P =

0.09), respectively. These two dates can be combined in a weighted mean age of **3544 ± [26] Ma** (MSWD = 0.38; P = 0.54; Fig. 5). Note that for each weighted mean age, we include the mini-plateau ages only because they are statistically agreed with the plateau ages (cf. discussion by Jourdan, 2012).

The K/Ca plots for each fragment are given in Annex 2. In general, the analyses show that higher-K domains degassed at low temperatures, while lower-K (higher Ca) reservoirs degassed at higher temperatures, which is typical behavior for both extraterrestrial and terrestrial basaltic rocks (e.g., Bogard, 2011; Jourdan et al., 2012). There is however, a subtle difference in degassing behavior between the coarse- and fine-grained aliquots. For the coarser material the K/Ca values decrease fairly steadily from low to high temperatures. On the other hand, analyses of the finer grained material have 'hump' shaped K/Ca release spectra, with the highest K/Ca values being at mid temperatures, with lower K/Ca at low temperatures, and the lowest K/Ca at high temperatures (Annex 2). These compositional variations are not commensurate with any $^{40}Ar/^{39}Ar$ age variation, giving us confidence that the ages recorded by each of the fractions were produced by real geological events.

Most of the age spectra show younger ages for the first few % to few tens of % of the total ^{39}Ar released. Following Shuster et al., (2010), we plotted the young low-temperature steps that departed from plateaus for both coarse- and fine-grained samples (Fig. 4). Remarkably, all the steps are statistically indistinguishable (P = 0.11) and can be combined in a weighted mean (apparent) age of 3419 ± [23] Ma. The significance of this apparent age will be described in more detail in the discussion section.

As stated above, inverse isochron plots (not shown) indicate that the data are systematically highly clustered near the radiogenic ($^{40}Ar^*/^{39}Ar$) axis showing that virtually no trapped ^{40}Ar is present in the system. As such, the inverse isochron cannot be used to estimate the value of any trapped Ar but, on the other hand, this makes the age calculation completely insensitive to

the $^{40}Ar/^{36}Ar$ value chosen for the trapped ratio (in this study, we use the standard cosmic value of 1 ± 1; Korochantseva et al., 2007).

Exposure ages:

Only five apparent dates of 4 ± 4 Ma, 4 ± 8 Ma; 18 ± 19 Ma; 20 ± 63 and 37 ± 72 Ma were obtained. However, it is unlikely that these apparent ages have any geological significance as (1) they were calculated based on very low ^{38}Ar ion beam signals relative to ^{40}Ar, ^{39}Ar and ^{37}Ar (Annex 1) and (2) none of the data from the particles showed any spread along the cosmochron, but rather a cluster of overlapping points. Rather, these data should be interpreted as indicating a very young exposure age for the Bunburra meteorite, in accordance with the ~21 Ma CRE age results of Welten et al. (2012).

$^{40}Ar/^{39}Ar$ results: Fusion crust

$^{40}Ar/^{39}Ar$ step heating analyses of four individual fragments of fusion crust yielded apparent inverse isochron ages ranging from 0 Ma (i.e., impossible positive isochron slope) to 768 ± 710 Ma, essentially indistinguishable from a zero age (Fig. 7). Most of the heating steps in the inverse isochron diagram cluster near the trapped argon y-axis and yield $^{40}Ar/^{36}Ar$ values ranging from ~294 to 321 ± 31 and are thus indistinguishable from the atmospheric $^{40}Ar/^{36}Ar$ ratio of ~298.6 ± 0.1 (Lee et al., 2006). These fusion crust fragments have K/Ca values that are homogenous with no variation from low to high step-heating temperatures (Fig. 8), indicating that the pyroxene and plagioclase minerals that were responsible for the variable K/Ca ratios in the groundmass were melted and turned into homogenous glass. However, one glass chip (SG-1; Fig. 8) shows a very different signature with an apparent age of 2.4 ± 0.5

Ga, sub-atmospheric trapped $^{40}Ar/^{36}Ar$ ratio of 211 ± 56 (Fig. 7) and heterogeneous K/Ca spectrum (Fig. 8).

Discussion

Significance of the ~3.64 Ga $^{40}Ar/^{39}Ar$ age: an impact event.

The K/Ar system is particularly sensitive to post-formation heating events above a couple of hundred of degrees (cf. below). Such conditions are usually met during hypervelocity asteroid impact events (Boggard, 1995). Depending the energy of the impact and the P-T conditions triggered by the impact at the sample site, part of the pre-existing radiogenic $^{40}Ar^*$ accumulated prior the impact event may be purged from the system (Jourdan et al., 2007). In this case, $^{40}Ar/^{39}Ar$ measurements will reveal a typical argon diffusion loss profile (i.e., $^{40}Ar/^{39}Ar$ age spectra with a logarithmic shape; (McDougall and Harrison, 1999)). Eventually, if an impact is sufficiently energetic, all previous $^{40}Ar^*$ is removed from the system and the K/Ar clock is reset at the time of the impact. If no other heating event occurs after that, melt rocks and shocked minerals from the target rock will exhibit flat $^{40}Ar/^{39}Ar$ age spectra (i.e. ~100% plateaus). The Bunburra meteorite yielded seven well-defined plateau ages (Fig. 2 and 3) with concordant ages (P = 0.53) from which a weighted-mean age of 3640 ± [21] Ma could be calculated (Fig. 4). Altogether, the well-defined plateaus, the absence of co-variation between apparent step ages and K/Ca (Annex 2), and the reproducibility between plateau ages suggest that this age reflects a true geological event at ~3.64 Ga. The relatively young ages of the breccia lithologies suggest that the 3.64 Ga $^{40}Ar/^{39}Ar$ age is not linked with volcanic activity on the Bunburra parent body. Therefore, the event that reset the K/Ar system of the Bunburra meteorite is likely related to a heating event caused by a sufficiently energetic (i.e.

~large) impact on the Bunburra parent asteroid. The magnitude of this impact is difficult to constrain based only on chronological studies but we now know that the K/Ar, Pb-Pb and Al-Mg radioisotopic chronometers were all variably affected by this event (this study, Spivak-Birndorf et al., 2010). A combination of petrographic observations and Ar diffusion models may help to shed light on the magnitude of the event.

Testing the temperature conditions at the time of impact

The $^{40}Ar/^{39}Ar$ systematics of the Bunburra achondrite imply that the temperature was high enough and for sufficient duration to diffuse ^{40}Ar completely out of the Bunburra parent rock. In order to provide a quantitative estimate for the impact temperature, it is necessary to determine whether (1) the Bunburra meteorite is an impact breccia made of primary basalt fragments that have been totally degassed of their $^{40}Ar^*$ upon impact, or (2) if the impact was energetic enough to cause complete fusion of the basaltic target rock and erase all sign of shock (e.g., the Manicouagan and Popigai impact melt sheets; French, 1998). In case (2), the breccia fragments would come from various part of a melt rock sheet with a basaltic composition. Upon relatively slow cooling, this melt would have crystallized plagioclase and pyroxene crystals. In such a hypothesis, a subsequent smaller impact would have brecciated the melt rock and brought together pieces with different grain sizes without significantly affecting the K/Ar system.

1. Diffusion models

The Bunburra meteorite petrology shows limited signs of shock (Fig. 1). If hypothesis (1) is valid, this implies that the temperature and pressure were low enough that they did not reach

localized melting conditions as there is no sign of melt veins, nor maskelynite (cf. El Goresy et al., (2013) for definition of maskeleynite as adopted in this study). Neither the P-T conditions were met to form diaplectic glass (P= 25-35 GPa ≈ 600 °C for basalt). Nevertheless undulatory features and cracks were observed suggesting temperatures around 200-300°C and pressures of 10-20 GPa (French, 1998; Langenhorst and Deutsch, 2012; Gillet and El Goresy, 2013). Therefore, the first hypothesis would require moderately elevated temperatures sustained for long enough to fully reset both plagioclase and pyroxene crystals. To test this hypothesis, we used the diffusion equations of Crank and Gupta (1975) for a sphere with a 150 μm radius and for fractional Ar loss between 85 and 100%. A radius of 150 μm is consistent with the crystal sizes of Bunburra, although we note that the true diffusion radius of the basalt sheet is in reality unknown. Specifically, we test the temperature (T) and time (t) conditions required to reset plagioclase and pyroxene crystals as well as a basaltic melt used as a proxy for solid basalt rock. Recently, Cassata et al. (2009) and Cassata and Renne (2013) have demonstrated that the diffusion parameters of plagioclase are variable and Cassata and Renne (2013) concluded that "there is no broadly applicable set of Ar diffusion parameters that can be utilized in thermal modelling". In this study, we use D_0 (pre-exponential factor) and E_a (activation energy) values of 4.98×10^{-2} cm²/s and 196 kJ/mol derived from the value measured by Cassata and Renne (2013) for lunar anorthitic plagioclase. The D_0 value was calculated from the $\ln(D_0/a^2)$ value of 5.4 $\ln(s^{-1})$ published by Cassata et al. (2013) and using a grain radius of 150 μm for the present study. We note that, in reality, the large range of D_0 and E_a values gives variable solutions for plagioclase. Similarly, Weirich et al. (2013) have demonstrated that pre-existing shock levels substantially increase the argon diffusivity in plagioclase during subsequent shock events, although we note that petrographic observations suggest that Bunburra crystals are unshocked. Nevertheless, because of all the possible

variation in the diffusion parameters, our diffusion models should be considered semi-quantitative only.

Similarly, for pyroxene a large range of diffusion values has been proposed (e.g., Cassata et al., 2010, Cassata et al., 2011, Weirich et al., 2012). In this study, we use $\ln(D_0/a^2) = 12.4\ s^{-1}$ ($D_0 = 5.46 \times 10^1$ cm²/s) and $E_a = 356$ kJ/mol obtained by Cassata et al. (2011) for pyroxene CPX-12 and calculated here for a radius of 150 µm. In comparison, we also modelled a somewhat "leaky" pyroxene with values of $D_0 = 7.1 \times 10^4$ cm²/s and $E_a = 377$ kJ/mol, taken as intermediate values from the range of values measured by Weirich et al. (2012) and calculated for a radius of 150 µm. We used $D_0 = 4.5 \times 10^1$ cm²/s and $E_a = 257$ kJ/mol for basaltic melt (Nowak et al., 2004). We also model the diffusion of Pb in pyroxene using $D_0 = 3.8 \times 10^{-1}$ cm²/s and $E_a = 372$ kJ/mol (Cherniak, 1998) in order to better understand the relation between our $^{40}Ar/^{39}Ar$ results and the Pb-Pb results of Spivak-Birndorf et al. (2010) based on plagioclase and pyroxene that gave perturbed results. Results are presented as T-t total-reset curves in Fig. 9, where a total Ar* reset is achieved when the system crosses a curve for a given mineral toward the right of the diagram (Jourdan et al., 2007; Jourdan et al., 2010).

Our calculations show that plagioclase and pyroxene crystals heated at a constant temperature of 1000°C are fully reset in ~122 hours and ~48 years, respectively, whereas a particle of basaltic melt will be reset in ~44 hours (Fig. 9). A leaky pyroxene would be reset in ~3 months. Note that these numbers are strict minima because in a real system, a ^{40}Ar atom is not necessarily lost once it has escaped a crystal, as it can remain trapped in a matrix of neighbouring crystals (hence diffusing into adjacent crystals). In addition, the diffusion length in the target rock can be much larger than the 150 µm grain radius adopted here and as said above, the diffusion parameters vary greatly for a given mineral. Even taking into account the fact that the model offers minimum time and temperature limit solutions, Fig. 9 shows that

high temperatures sustained for a relatively long period of time are required to reset both pyroxene and plagioclase.

An A-T-t curve (Jourdan et al., 2007; Jourdan et al., 2010) represents the relative inherited ^{40}Ar* concentration (A) – temperature (T) – time (t) history of a given crystal or melt rock grain. For the purpose of this study, we are not interested so much in the amount of ^{40}Ar* left in the system but whether a crystal or grain achieves total Ar* reset (Fig. 2 and 3). If an A-T-t curve crosscuts a mineral total-reset curve, it implies that the thermal history of the rocks was sufficient to fully reset this mineral. Fig. 9a shows an A-T-t path (black dashed curve #1) where a crystal is heated to 1000°C for 100 hours, after which the system cools down and reaches a relative equilibrium temperature of 700°C over 120 hours. These conditions are sufficient to reset the basaltic groundmass, but not the plagioclase or pyroxene crystals. Such an A-T-t path is admittedly arbitrary and probably excessive according to petrographic observations, but it illustrates the extreme conditions required to fully reset pyroxene or plagioclase crystals at solid-state conditions. High impact temperatures above 1000°C sustained for more than a few seconds to at best a few hours, especially when associated with initial shock pressure of few tens of GPa, are enough to irreversibly transform (i.e, PDFs, diaplectic glass) the crystals within the target rock (French, 1998; Langenhorst and Deutsch, 2012; Gillet and El Goresy, 2013). Again, these conditions are largely above the P-T conditions estimated from petrographic observations. Nevertheless, although petrographic observations suggest low shock levels (and by correlation low temperatures), parameters such as porosity can play a significant role in shifting the Hugoniot curve (i.e. a non isothermal curve relating temperature and pressure during shock metamorphism; Langenhorst and Deutsch, 2012) toward high temperatures for relatively low shock level. Therefore, we tested if the K/Ar system of the Bunburra meteorite could have been reset by solid-state diffusion for

temperatures well within excess of the temperature range estimated from petrographic observations alone.

2. Hypothesis 1: solid state diffusion upon impact

At temperatures of 1400-1500°C, a given doleritic or gabbroic target rock made of plagioclase and pyroxene crystals will show sign of localized melting around the crystal edges as constrained by the solidus temperature of anorthitic plagioclase and pyroxene (McBirney, 1984; Spray, 2010). An average of 1250°C is generally given for the solidus temperature of gabbro (McBirney, 1984). However, the solidus temperatures also depend on pressure and, along the Hugoniot curve for basalt, the onset of melting will occur for temperatures of 1750°C corresponding to pressure of ca. 70 GPa (Gillet and El Goresy, 2013). For gabbro, the pressure value of the liquidus is slightly higher at 80 GPa. Nevertheless, it should be taken into account that basalt, pyroxene and plagioclase solidus temperatures are dependent on the total energy of the system per time unit to achieve melting. In other words, the temperature required to melt or partially melt a target mineral or rock is proportional to the time during which the heat is applied to this system. More energy (and hence higher temperature) is needed to melt a crystal when the energy is applied for 0.1s rather than 100s. At these very short timescales, the standard rules of equilibrium or partial melting for a two-component magmatic system do not apply for impact melting (Keil et al., 1997). We developed a series of time-temperature thermodynamic equations (Annex 3) that depicts the relationship between the time and temperature required for plagioclase to show signs of melting. The final equation of state can be written as:

$$t = \frac{c.\rho.V}{h.A} \ln \frac{T_f - T_0}{T_f - T_m} \quad (1)$$

where ***h*** is the heat transfer coefficient of the external fluid (W/m^2.K), A is the surface area of spherical plagioclase particles in m^2, ***V*** is the volume of these spheres in m^3, ***c*** is the specific heat capacity (kJ/kg.K), and ρ is the density of plagioclase (kg/m^3). Time (**t**) is given in seconds and the temperature of the external molten basaltic fluid ($\mathbf{T_f}$) is given in Kelvin. Initial temperature of plagioclase particles ($\mathbf{T_0}$) at time zero is taken as 123.15 K based the average surface temperature of the asteroid, while the melting temperature of plagioclase ($\mathbf{T_m}$) is around 1773.15 K.

The T-t solidus area for plagioclase is shown in Fig. 10. The calculated temperature-time solidus curve shows that plagioclase melting is unlikely to occur, even for high temperatures of a few thousand degrees if such temperatures are maintained for only few hundredths or tenths of a second. A-T-t paths for such high-temperatures and sustained for a short duration of a few tenths of a second before rapidly cooling down (e.g., A-T-t path #2 on Fig. 9a) show that, although temperature conditions just below the solidus might be sufficient to totally reset pyroxene, they would be far from able to reset plagioclase, even for temperatures of 3500°C (Fig. 10). Importantly, these curves show that none of the possible scenarios involving brief temperature spikes of a few thousand of degrees will be sufficient to reset pyroxene *and* plagioclase crystals without partially melting these minerals (Gillet and El Goresy, 2013). Borderline cases would be perhaps temperatures above 3600°C (Fig. 10) or a temperature of 1200°C, just below the eutectic temperature of gabbro (McBirney, 1984) and applied for at least between 18 hours for a leaky pyroxene to 6 month for a more conventional pyroxene, but again, no solid state transformation is observed in the Bunburra meteorite, precluding that such conditions ever occurred. These conditions are also far from being able to reset the Pb in

pyroxene (Fig. 9a and 10). Therefore, we conclude that brief heating conditions required to totally reset the system (both plagioclase and pyroxene) are *not* compatible with the lack of melt occurrences in the Bunburra meteorite (Fig. 1; Benedix et al., 2010).

3. Hypothesis 1: Solid state diffusion during slow cooling

Following a rapid temperature drop from the peak temperature, target rock equilibrium temperatures of ~1000-1100°C in the case of a melt rock are generally reached in a relatively short period of time of a few tens of seconds up to several thousand years (i.e., depending on a variety of parameters such as position in the melt sheet and type of rock; Onorato et al., 1978; Keil et al., 1997). Equilibrium temperatures are more likely around 700-800°C if the rock and its components remained sub-solidus. Recent $^{40}Ar/^{39}Ar$ analyses of plagioclase from the terrestrial Lappajarvi impact structure by Schmieder and Jourdan (2013) suggest that subsequent cooling from equilibrium temperatures (ca. 1000-1100°C) down to below ca. 200°C can happen over a significantly longer period than initially estimated by theoretical calculations alone. These authors showed that it can take between 0.5 and 1.5 Ma for a relatively small (24 km in diameter) craters to cool down below ca. 200 °C. Whether the Bunburra meteorite also records such an extended cooling duration is hard to tell in particular relatively to the small mass of the parent relative to Earth, and the faster cooling of the melt due to the lower surface temperatures (since the temperature at the surface of an asteroid in the asteroid belt is in average significantly lower than on Earth, due to its greater distance to the sun and the absence of buffering atmosphere). As such, this model must be taken as a test for an extreme case scenario. We modelled the effect of the temperature of a relatively slow cooling target on the Ar* diffusion in pyroxene, plagioclase and basalt. We used the same diffusion parameters as mentioned previously, and used a slow cooling gradient of 500°C/Ma

for the A-T-t path taken from Schmieder and Jourdan, (2013). These values ensure that we test a scenario where the proportion of argon loss is somewhat a maximum value. Our calculations show that these time-temperature conditions are in fact sufficient to fully reset plagioclase and basalt by slow diffusion, but are not sufficient to reset pyroxene (Fig. 9b). Although a pyroxene crystal will lose its Ar* much faster than plagioclase at relatively high temperatures, it will be extremely resilient to low temperature diffusion (Cassata et al., 2010). In our model, the temperature of the kinetic cross-over between pyroxene and plagioclase (i.e., the temperature below which plagioclase will diffuse faster than pyroxene in a T-t graph) for total Ar loss will occur at a temperature of ~2500°C for pyroxene and ~1300°C for leaky pyroxene (Fig. 9a). As shown by the $^{40}Ar/^{39}Ar$ spectra, the high-temperature (Ca-rich) part of the spectra that mostly include pyroxene shows no departure from plateaus, demonstrating that pyroxene crystals have been fully reset as well. Nevertheless, in the extreme case of an equilibration temperature of 900°C, all minerals would be reset during slow cooling (Fig. 9b). Alternatively, a high temperature spike below the solidus followed by a slow cooling might reset both pyroxene and plagioclase. We also note that none of these conditions are close to allow resetting the Pb-Pb chronometer in pyroxene, which would require sustained temperatures in excess of 1100°C for more than 1 Ma (not shown). As such, the Pb-Pb is more likely to be disturbed rather fully reset. Temperature conditions required to reset the ^{40}Ar both in pyroxene and plagioclase would be sufficient to form diaplectic glass (900 – 700 °C; (French, 1998; Langenhorst and Deutsch, 2012), which is not observed in the Bunburra meteorite.

To illustrate the effects of some of the previous time-temperature conditions on a $^{40}Ar/^{39}Ar$ age spectrum, we used an upgraded (Forster and Lister, 2010) version of the program MacArgon (Lister and Baldwin, 1996) to simulate the effect of a given A-T-t path of a dolerite target rock made of 60% plagioclase and 40% of pyroxene. The diffusion parameters

are the ones used for plagioclase and leaky pyroxene. We simulate a 3.6 Ga event on a 4.5 Ga target rock, with temperature of 1000°C sustained for a duration of 100 hours (Fig. 11a). We also simulate similar conditions followed by a relatively slow cooling of 500°C/Ma (Fig. 11b). Both simulations did not achieve a full reset of inherited $^{40}Ar^*$ and show structured synthetic age spectra. Both spectra show hump-shaped patterns where the age spectrum of Fig. 11b (where the simulation include a cooling period) is more depleted in $^{40}Ar^*$, than in the case of the high temperature event alone. The hump shaped pattern is due to the different diffusion characteristics between pyroxene and plagioclase, where plagioclase has lost more of its $^{40}Ar^*$ than pyroxene at temperatures below the kinetic cross-over temperature (here calculated to be ca. 1300°C between plagioclase and leaky pyroxene; Fig. 9). The characteristics of diffusion of these models imply that plagioclase is more depleted than pyroxene. They also imply that during a $^{40}Ar/^{39}Ar$ step-heating experiment in the laboratory, the release of argon from the plagioclase contributes to most of the $^{40}Ar/^{39}Ar$ spectrum (a wide degassing curve covering all the temperature range) whereas pyroxene will significantly contribute to a more restricted part of the age spectrum (mostly 30-90 % of ^{39}Ar released). These numerical models, even taking the least favorable diffusion parameters of the leaky pyroxene, confirm our previous calculations (Fig. 9) and confirm that the T-t conditions met during the Bunburra impacts would not be sufficient to fully reset the K/Ar system without being close to melting conditions and producing irreversible petrographic changes in the target rock (French, 1998; Langenhorst and Deutsch, 2012).

4. Hypothesis 2: complete melting of a basaltic target rock

Shock melting of the parent target rock would be a straightforward mechanism to explain the full reset of the K/Ar system and the disturbance of the Al-Mg and Pb-Pb systematics

found in Bunburra (Spivak-Birndorf et al., 2010). At temperatures of a few thousand degrees, a basaltic / doleritic target rock is fully melted in less than a few seconds (Fig. 10). At melt condition (above the liquidus), A-T-t calculations show that a basaltic melt particle will be purged of all its inherited $^{40}Ar^*$ in only 0.06 second at a temperature of 3000 °C. At a temperature of 5000°C, the same result is achieved in only 0.002 second. The important thing to consider in these calculations is that the relatively slow-diffusing plagioclase does not exist in the melt state and the plagioclase and pyroxene diffusion curves collapse into the molten basalt curve shown in Fig. 9a. The diffusion characteristics of liquid basalt imply that a molten basaltic fragment is far more prone to diffusion than a solid plagioclase crystal (Fig. 9a). In reality, the true diffusion length scale of a melt sheet will be bigger than the 150 micron radius adopted in this study, but this might be partially compensated by advection (i.e. direct matter transportation) which is also likely to play an important role in terms of Ar loss mechanism from the melt. Based on the lack of significant shock features and localized fusion, and considering the difficulty in fully purging Ar from solid crystals of plagioclase and pyroxene crystals compared to molten basalt, we suggest that the Bunburra meteorite basalt was formed following an impact event that had sufficient energy to entirely melt the basaltic target rock. Subsequent to the impact, relatively slow cooling allowed pyroxene and plagioclase to crystallize within the melt rock.

Furthermore, using the Pb diffusion characteristics of pyroxene (Cherniak, 1998) and assuming that pyroxene melts have Pb diffusion characteristics close to pyroxene crystals (e.g., this has been demonstrated at least for Ar and CO_2 in compositionally variable silicate melts; Nowak et al. 2004), our model shows that even at melt conditions, Pb will be very slow to diffuse out of the melt particle (Fig. 9a and 10). In reality, if the target rock was completely melted, then open system behaviour would be required to change the whole-rock Pb isotope systematics of a given portion of the melt sheet. This could only be achieved by volatile loss

(degassing) of Pb or by melt segregation and re-crystallization (U-Pb fractionation), but the latter processes are far harder to model than Pb diffusion in a single grain of pyroxene. Therefore, what our model truly indicates is that the Pb-Pb chronometer, in particular when compared to the K/Ar chronometer, will be resilient to impact resetting and it follows that only very energetic (and by extrapolation large) impacts will reach T-t conditions sufficient to fully reset the Pb-Pb systematics on a global scale.

$^{40}Ar/^{39}Ar$ analyses of the fusion crust of the Bunburra meteorite brings some independent evidence to support an extremely fast diffusion of $^{40}Ar^*$ in liquid basalt compared to the crystal solid state. The invariant K/Ca ratios (Fig. 8) of four glass aliquots show that both pyroxene and plagioclase crystals have been completely molten and mixed into a homogenous glass. These aliquots yielded apparent ages indistinguishable from 0 Ma and trapped argon with a $^{40}Ar/^{36}Ar$ composition indistinguishable from atmospheric argon ($^{40}Ar/^{36}Ar$ = 299; Lee et al., 2006) that was incorporated during atmospheric travel. This demonstrates that all the $^{40}Ar^*$ has been removed from the glass during fusion. A fifth aliquot shows a different behavior with an apparent age of 2.4 ± 0.5 Ga, a trapped $^{40}Ar/^{36}Ar$ ratio of 211 ± 56, and a heterogenous K/Ca ratio (SG-1 in Fig. 8). A variable K/Ca ratio suggests that the crystals were not completely molten and that the fusion crust still contained some plagioclase and/or pyroxene crystals. This is in agreement with an apparent old age, which is probably intermediate between the 3.6 Ga $^{40}Ar/^{39}Ar$ age of the Bunburra meteorite and zero age of the fall. This is also in agreement with a sub-atmospheric ratio as a mixture from the $^{40}Ar/^{36}Ar$ ratio of the meteorite (cosmogenic value of ~1) with the atmosphere (~299). Interestingly, although the T-t path of the fusion crust is hard to constrain, the Ar results show that solid crystals embedded within a basaltic melt at more than 1500°C will diffuse $^{40}Ar^*$ much more slowly than the melt, in accordance with our diffusion model curves (Fig. 9).

Previous $^{40}Ar/^{39}Ar$ and $^{40}Ar/^{36}Ar$ measurements of fresh ~0.5 Ma basaltic melt rock from the Lonar crater (India) emplaced in the ~66 Ma Deccan basalts showed that, once the liquidus (i.e. complete melting) is reached, all inherited Ar is quickly and completely purged from the basaltic melt rock (Jourdan et al., 2011). Interestingly, Lonar is a very small crater of ca. 2 km in diameter (Fredriksson et al., 1973). This means that, as long as the basalt liquidus is reached, the K/Ar system of a basaltic target rock can be reset regardless the size of the crater, although admittedly, local conditions of the melt sheet are likely to play a role as well in this process. Normal aphyric basalt liquidus temperatures are on the order of 1250°C (McBirney, 1984), whereas melting of plagioclase and pyroxene crystals require higher temperature of ca. 1400-1500°C (McBirney, 1984; Spray, 2010). More realistically and as mentioned above, higher energy densities (and hence temperatures) per time unit are needed to fully melt a rock in a short spike with a duration of a few tenths of a second to a few seconds (Fig. 10). This means that if such melting conditions can be easily reached for a small impact like Lonar, a full reset of the Ar system is therefore not indicative of a large crater size, and is likely to be very common on basaltic target rocks throughout the solar system. Note that if for some reason the target rock is porous (e.g. basaltic regolith) then even lower impact energy is required to melt such a target rock (Keil et al., 1997; Wünnemann et al., 2008). Nevertheless, the Bunburra meteorite has well-developed crystals of pyroxene and plagioclase up to hundreds of microns long, which contrast with the aphyric Lonar melt rocks (Osae et al., 2005). The crystalline nature of Bunburra indicates much slower cooling (and hence, a larger impact) as compared to Lonar, and is instead similar to the texture of the noritic impact melt of the Sudbury basin (Therriaut et al., 2002).

In summary, based on the $^{40}Ar/^{39}Ar$ data of Bunburra groundmass and fusion crust fragments and diffusion models at solid-state and melt conditions, we conclude that the Bunburra basaltic achondrite is mostly made of melt rock fragments formed at 3.64 Ga by a

medium to large impact event. However, this impact was not sufficient to fully equilibrate the Pb isotopes amongst mineral phases and only partially disturbed the Pb-Pb chronometer ages.

Timing of the breccia formation.

Whereas the Bunburra melt rock was fully reset during the ~3.64 Ga impact, a secondary event is required to fragment and recombine pieces of the melt rock containing crystals with various grain sizes. It is not clear if a tertiary impact is required to weld all the clasts together into a breccia or rather if this was achieved during the fragmentation event.

As demonstrated above, solid state diffusion without melting is unlikely to fully reset the K/Ar system in basalt and the brecciation event is unlikely to be the one that reset the Bunburra melt rock at 3.64 Ga. Nevertheless, sub-solidus heating events, even if not crossing the Ar reset curves (Fig 9) will cause a portion of the ^{40}Ar* to diffuse out of the system (cf. examples in Jourdan et al., 2007). For example, using the diffusion parameters indicated above, a basalt fragment will be fully reset in 44 h at 1000°C but will lose only 15% of its ^{40}Ar* if heated at the same temperature for 10 minutes. The latter sample would exhibit a ^{40}Ar/^{39}Ar age spectrum with a characteristic log-shaped Fickian diffusion profile (McDougall and Harrison, 1999). Such small heating events still allow recovering a formation age provided that a plateau including at least 70% of the gas released is achieved. Below a threshold of 70% gas release, all crystal domains including the ones forming the flat section of a spectrum are affected to some extent by ^{40}Ar* diffusive loss. Such mini-plateaus and sub mini-plateaus are therefore only indicative of a strict minimum formation age (see empirical data on plagioclase from the Bushveld complex shown by Cassata et al. (2009) and discussion by Jourdan (2012)).

An important question is whether we can use low temperature apparent ages (i.e., youngest ages located at the left of the age spectra; Fig. 2 and 3) of Fickian diffusion profiles to derive ages for small secondary events. In theory, argon released in the lowest temperature steps comes from plagioclase and should be able to reach the age of the secondary heating event (cf. the low temperature steps of the synthetic age spectra presented in Fig. 11), but in practise, it is not necessarily the case. First, the $^{40}Ar/^{39}Ar$ step-heating process follows a step-function rather than a true extraction continuum and thus averages the age of the low temperature steps of a given spectrum. In addition, 1-2% argon can also be lost during irradiation and bake out procedures. Hence, low temperature steps tend to provide only a *maximum* age for small secondary heating events. Recent thermochronogical analyses of a set of logarithmic-shaped $^{40}Ar/^{39}Ar$ age spectra obtained on lunar regolith rocks by Shuster et al. (2010) suggest that in this particular case, it can be demonstrated that age spectra fully recorded the age of a ~3.3 Ga secondary heating event in their low temperature extraction steps. In the case of the Bunburra meteorite, the fact that nine aliquots with two different average grain sizes (coarse and fine) and from different locations in the meteorite all yielded a total of twenty-four low temperature steps with statistically indistinguishable ages (P=0.11; Fig. 6) suggests that each sample had its low temperature domains fully reset at the time of a secondary event. This may suggest that the age of the impact responsible for the fragmentation of the target rocks and/or amalgamation of the Bunburra meteorite breccia is constrained at 3419 ± [23] Ma (Fig. 6). Deriving A-T-t constraints for the breccia during this impact is not straightforward. The A (i.e., Ar*) parameter can be estimated based on the shape of the age spectra assuming a formation age of 3.64 Ga (melting event) and a secondary impact at 3.42 Ga (brecciation event). With spectra shapes resembling a two-step function rather than true Fickian diffusion profiles, one can estimate a $^{40}Ar^*$ loss of 10-20% at the time of the event. Since argon diffusion is probably recorded only by plagioclase crystals in this part of the age spectrum, a

T-t pair cannot be calculated for this range of Ar* loss but only a co-variation curve with a fraction of argon loss of 15% (Fig. 10). Conversion of apparent shock features of ca. 30 GPa to temperature of ~500°C for basalt on the Hugoniot curve (Gillet and El Goresy, 2013) suggests that such a temperature should be maintained over 3.6 years in the breccia to remove 15% of ^{40}Ar* from the target rock. More importantly, Fig. 10 shows that the 15% ^{40}Ar* loss T-t curve stays below and never crosses the solidus of plagioclase and is in agreement with the lack of melting evidence and the absence of maskelynite due to the brecciation event.

Significance of the 3.54 Ga age.

Only two of the nine samples yielded ages of ~3.54 Ga (Fig. 2, 5 and Table 1). Whereas one sample produced only a borderline 51% ^{39}Ar released mini-plateau and could well be a datum artefact (cf. discussion by Jourdan (2012)), a second sample produced a robust 82% ^{39}Ar released plateau age with a P-value of 0.83. Therefore, based on the latter sample, there is a possibility that this piece of Bunburra recorded a true impact event at ~3.54 Ga. Both the plateau and mini-plateau ages were obtained on coarse breccia aliquots. We see three possible explanations for such an age: (1) the monomict breccia is in fact a polymict breccia including components of similar compositions that melted (and were reset) at 3.64 and 3.54 Ga respectively, and were brought together during the brecciation event at 3.42 Ga, (2) the age of the brecciation event is in fact constrained at 3.54 Ga and some part of the breccia recorded this event or (3) the brecciation event partially reset the K/Ar system that recorded the 3.64 Ga age and the 3.54 Ga age is an intermediate and meaningless date.

Hypothesis (3) can be dismissed as plagioclase and pyroxene would not be partially reset to the same intermediate age due to their vastly different diffusion characteristics and a plateau could not be formed (Kennedy et al., 2013). Hypothesis (2) is possible and would require that

some parts of the target rock would have been molten whereas some parts would have stayed solid and preserved the 3.64 Ga age. However, the 3.54 Ga age is recorded in the *coarse* breccia, which is expected to cool slowly and thus is not easily reconcilable with a fast cooling expected in the case of a mingling between cold and molten rocks. The polymict breccia hypothesis (1) offers an easy explanation. However, in this case, the term polymict does not imply that the target rocks had different compositions, but rather that a compositionally unique basaltic target rock (Fig. 1; Benedix et al., 2010) underwent different thermal histories. In the latter case, each of the ~3.64 and ~3.54 Ga cratering and melting events happened in close proximity on spatially extensive homogenous basaltic target rock. The ~3.64 and ~3.54 Ga melt rocks would have been excavated and brought together during the fragmentation/brecciation event at ~3.42 Ga. Although we feel that this scenario is convincing, it only relies on a single solid plateau age and is admittedly hard to test because of the lack of compositional variations between the different lithologies (Benedix et al., 2010).

Impacts at the surface of the Bunburra and HED primary and secondary parent bodies.

As demonstrated above, the 3.64 Ga and perhaps 3.54 Ga impact events generated sufficient energy to melt the basaltic target rock and thus fully reset the K/Ar chronometer. The occurrence of coarse grained melt rocks for both age populations requires that the two impacts were large enough to have caused a slowly cooling melt pond at the bottom of the crater. Unlike as observed on terrestrial craters, slow cooling on asteroids cannot be achieved below a certain crater size, because the cooling gradient between the surface of the asteroid and the melt pond would cause a thin sheet of melt to quench rapidly. Nevertheless, it is not clear how much of a difference this makes in the high temperature (i.e., near solidus) cooling history of the impact melt.

Therefore, both the A-T-t history of the rock and the presence of coarse grained melt rock cannot be used as diagnostic tool between medium-size and very large impacts at the surface of the Bunburra parent body, but seem to exclude a small (few kilometers in diameter) size crater.

A recent study by Kennedy et al. (2013), using exclusively well-defined $^{40}Ar/^{39}Ar$ plateau ages showed that the duration of the major impact activity at the surface of the HED parent body (thought to be asteroid 4 Vesta; (McSween et al., 2011) might be more restricted than previously thought (ca. 4.1 – 3.4 Ga; Bogard, 2011; Cohen, 2013; Marshi et al., 2013) and a very limited set of plateau age data currently available rather indicates that such activity occurred between ca. 3.5 and 3.8 Ga. Clearly, more well-defined plateau ages are required to get a comprehensive understanding of the timing of the bombardment history on Vesta as this restricted history can currently be due to a sampling bias, but adopting the complete age dataset based on statistically discordant age data (e.g. Marshi et al., 2013) is in many ways worse than a restricted number of robust ages (Kennedy et al., 2013; Jourdan, 2012). Nevertheless, it is interesting to see that, based on current data, most the bombardment activity on achondrite parent bodies concentrate in a short period of time. This is in stark contrast to how easy it is to reset the K/Ar system in basalts. Even the relatively small impact that formed the ca. 2 km in diameter Lonar crater was sufficient to completely reset the basaltic target rock (Jourdan et al., 2011). The lack of *well-developed* plagioclase or matrix plateau ages that post-date ~3.5 Ga (Kennedy et al., 2013) is intriguing. As such, the K/Ar system on basaltic asteroids is perhaps not best suited to record the age of large impact events, but rather the youngest recorded ages provide information about the timing of the cessation of any significant bombardment activity on an asteroid parent body(?). This problem is similar for instance to the occurrence of the HED unbrecciated eucrite population that shows distinct

$^{40}Ar/^{39}Ar$ ages no younger than ~4.5 Ga (Bogard, 1995; Bogard, 2011; Kennedy et al., 2013), but which is virtually unperturbed by any secondary impact events after that.

The chronology of the Bunburra meteorite and eucrites indicates that these meteorites were protected from further (significant) melting-event impacts after 3.5 Ga. This can be achieved in two different ways: minimal target size or shielding. The first possibility implies that a relatively small chunk of asteroid (secondary parent) containing the meteorite is ejected from a primary parent body during a large impact. The small target size and negligible gravity pull of the secondary parent would render the latter a target particularly difficult to hit by large and/or energetic impactors. Only small objects would regularly hit the small parent body, but the energy generated by those small impacts would be too low to reset the K/Ar chronometer. This scenario is tempting, although we note that it is in apparent contradiction with current orbital dynamic models of the asteroid belt that estimate a life span of several million of years for 10 km size asteroids (Bottke et al., 2005). The second possibility is that the Bunburra meteorite was shielded from impact heating by a protective blanket at least a few kilometers thick, and the specimen was excavated and liberated much later in the history of the parent body. In this scenario, the heat generated by impact events post 3.5-3.4 Ga is systematically absorbed by the porous protective blanket whereas the underlying consolidated breccia is pore-free and thus, requires much more energy to achieve the same temperature. The natural decrease of the frequency of bombardment might imply that impacts younger than 3.4 Ga become too small on average to generate sufficient energy to heat the porosity-free breccia protected by ultra-porous regolith. Nevertheless, it is not clear why *all* eucrites analyzed so far would have been protected under a blanket of ejecta for the last ~3.4 Ga and in the case of the unbrecciated eucrites, for the last ~4.5 Ga. Although this hypothesis is interesting, it requires further testing.

Finally we note that the impact history recorded by some of the brecciated eucrites (peak at 3.8-3.5 Ga according to Kennedy et al. (2013)) is similar to the impact history recorded by the Bunburra parent body (ca. 3.64-3.54 Ga; this study) but seems different than the histories given by various type of chondrites based on the available data (Swindle et al., 2014). This could indicate a similar position of the two differentiated parent bodies in the asteroid belt at that time. The fact that the oxygen isotope composition is different between anomalous eucrites and HEDs could imply that the Bunburra parent body was not accreted in this part of the asteroid belt but rather migrated there later, prior to 3.6 Ga.

Conclusions / summary

Based on $^{40}Ar/^{39}Ar$ results obtained on two lithologies of the Bunburra meteorite (Fig. 12) and fusion crust, previous Al-Mg and U-Pb results, argon diffusion models and comparison with a terrestrial analogue, we envisage the following scenario for the Bunburra Rockhole meteorite.

(1) Part of the pre-3.6 Ga bombardment history of Bunburra meteorite might still be recorded by the Pb-Pb system that yielded an apparent age around 4.2-4.1 Ga. However, the lack of statistically robust results does not allow us to confirm if this apparent age is meaningful or if it represents a partially reset age, intermediate between the 4.5 Ga formation age and the 3.6 Ga impact event. (2) A medium- to large-sized impact crater of perhaps tens of km in diameter or more occurred at 3640 ± [21] Ma Ga on Bunburra's parent body. The impact event had sufficient energy to melt part of the target rock and erase all preceding history from the K/Ar system, whereas the T-t history and open system behavior of the melt rock were not sufficient to completely erase the Pb-Pb age. Relatively slow cooling allowed crystals to grow up to several hundred of microns (forming coarse breccia). (3) A second

medium-size impact event might have occurred on a neighboring part of the same target rock at 3544 ± [22] Ma. This impact would have been sufficiently energetic to melt and reset the target rock while distal enough not to affect the ~3.64 Ga melt rock. (4) At ~3.42 Ga, a third impact excavated parts of the 3.64 (and 3.54) Ga melt rocks and brought together fragments with diverse grain sizes to form the coarse to fine breccia observed in the Bunburra meteorite. We consider the possibility that the third event was not sufficient to weld the fragments together and thus, a fourth impact (5) may be required. During this event (or perhaps shortly after) the Bunburra meteorite was either ejected and sat in a secondary, much smaller parent body where it stayed unperturbed for the last 3.42 Ga or was buried under a few kilometer thick protective regolith blanket during approximately the same duration. Finally, (6) Measured $^{38}Ar_c$ and $^{21}Ne_c$ CRE ages at ca. 21 Ma, indicating the final separation of Bunburra from its secondary (or higher order) parent body by a minor impact and before its entry into Earth's atmosphere in 2007.

Acknowledgements.

We acknowledge formal reviews by B. Cassata and two anonymous reviewers. We thank C. Hall for efficient editorial handling.

References

Benedix, G.K., Bland, P.A., Howard, K.T., Spurny, P., Bevan, A.W.R., 2010. The Mineralogy and Petrology of Bunburra Rockhole, Lunar and Planetary Institute Science Conference Abstracts, p. 1438.

Bland, P.A., Spurný, P., Towner, M.C., Bevan, A.W.R., Singleton, A.T., Bottke Jr, W.F., Greenwood, R.C., Chesley, S.R., Shrbený, L., Borovička, J., Ceplecha, Z., McClafferty, T.P., Vaughan, D., Benedix, G.K., Deacon, G., Howard, K.T., Franchi, L.A., Hough, R.M., 2009. An anomalous basaltic meteorite from the innermost main belt. Science 325, 1525-1527.

Bogard, D.D., 1995. Impact ages of meteorites: a synthesis. Meteoritics 30, 244-268.

Bogard, D.D., 2011. K-Ar ages of meteorites: Clues to parent-body thermal histories. Chem Erde-Geochem 71, 207-226.

Bottke, W.F., Durda, D., Nesvorńy, D., Jedicke, R., Morbidelli, A., Vokrouhlicḱy, D., Levison, H., 2005. The origin and evolution of stony meteorites, pp. 357-374.

Burbine, T.H., Buchanan, P.C., Binzel, R.P., Bus, S.J., Hiroi, T., Hinrichs, J.L., Meibom, A., McCoy, T.J., 2001. Vesta, Vestoids, and the howardite, eucrite, diogenite group: Relationships and the origin of spectral differences. Meteoritics & Planetary Science 36, 761-781.

Cassata, W.S., Renne, P.R., Shuster, D.L., 2009. Argon diffusion in plagioclase and implications for thermochronometry: A case study from the Bushveld Complex, South Africa. Geochim Cosmochim Ac 73, 6600-6612.

Cassata, W.S., Shuster, D.L., Renne, P.R., Weiss, B.P., 2010. Evidence for shock heating and constraints on Martian surface temperatures revealed by Ar-40/Ar-39 thermochronometry of Martian meteorites. Geochim Cosmochim Ac 74, 6900-6920.

Cherniak, D.J., 1998. Pb diffusion in clinopyroxene. Chem Geol 150, 105-117.

Clayton, R.N., Mayeda, T.K., 1996. Oxygen isotope studies of achondrites. Geochim Cosmochim Ac 60, 1999-2017.

Crank, J., Gupta, R.S., 1975. Isotherm Migration Method in 2 Dimensions. Int J Heat Mass Tran 18, 1101-1107.

Duffard, R., 2009. Basaltic asteroids in the solar system. Earth, Moon and Planets 105, 221-226.

El Goresy, A., Gillet, P., Miyahara, M., Ohtani, E., Ozawa, S., Beck, P., Montagnac, G., 2013. Shock-induced deformation of Shergottites: Shock-pressures and perturbations of magmatic ages on Mars. Geochim Cosmochim Ac 101, 233-262.

Eugster, O., Michel, T., 1995. Common Asteroid Break-up Events of Eucrites, Diogenites, and Howardites and Cosmic-Ray Production-Rates for Noble-Gases in Achondrites. Geochim Cosmochim Ac 59, 177-199.

Forster, M.A., Lister, G.S., 2010. Argon enters the retentive zone: Reassessment of diffusion parameters for K-feldspar in the South Cyclades Shear Zone, Ios, Greece, pp. 17-34.

Fredriksson, K., Dube, A., Milton, D.J., Balasundaram, M.S., 1973. Lonar Lake, India: An impact Crater in basalt. Science 180, 862-864.

French, B., 1998. Traces of Catastrophe: A Handbook of Shock-Metamorphic Effects in Terrestrial MeteoriteImpact Structures., in: Institute, L.a.P. (Ed.), LPI Contribution No. 954. LPI, Houston, p. 120.

Gillet, P., Goresy, A.E., 2013. Shock Events in the Solar System: The Message from Minerals in Terrestrial Planets and Asteroids. Annual Review of Earth and Planetary Sciences 41, 257-285.

Greenwood, R.C., Franchi, I.A., Jambon, A., Buchan, P.C., 2005. Widespread magma oceans on asteroidal bodies in the Early solar system. Nature 435, 916-918.

Greenwood, R.C., Barrat, J.A., Scott, E.R.D., Franchi, I.A., Yamaguchi, A., Gibson, J.M., Haack, H., Lorenz, C.A., Ivanova, M.A., Bevan, A., 2013. Large-Scale Melting and Impact Mixing on Early-Formed Asteroids: Evidence from High-Precision Oxygen Isotope Studies. LPI Contributions 1719, 3048.

Heymann, D., Mazor, E., Anders, E., 1968. Ages of calcium-rich achondrites-I. Eucrites. Geochim Cosmochim Ac 32, 1241-1268.

Jourdan, F., 2012. The Ar-40/Ar-39 dating technique applied to planetary sciences and terrestrial impacts. Aust J Earth Sci 59, 199-224.

Jourdan, F., Andreoli, M.A.G., McDonald, I., Maier, W.D., 2010. 40Ar/39Ar thermochronology of the fossil LL6-chondrite from the Morokweng crater, South Africa. Geochim Cosmochim Ac 74, 1734-1747.

Jourdan, F., Moynier, F., Koeberl, C., Eroglu, S., 2011. 40Ar/39Ar age of the Lonar crater and consequence for the geochronology of planetary impacts. Geology 39, 671-674.

Jourdan, F., Renne, P.R., 2007. Age calibration of the Fish Canyon sanidine Ar-40/Ar-39 dating standard using primary K-Ar standards. Geochim Cosmochim Ac 71, 387-402.

Jourdan, F., Renne, P.R., Reimold, W.U., 2007. The problem of inherited Ar-40* in dating impact glass by the Ar-40/Ar-39 method: Evidence from the Tswaing impact crater (South Africa). Geochim Cosmochim Ac 71, 1214-1231.

Jourdan, F., Sharp, W.D., Renne, P.R., 2012. Ar40/Ar39 ages for deep (~3.3 km) samples from the Hawaii Scientific Drilling Project, Mauna Kea volcano, Hawaii. Geochem Geophy Geosy 13.

Jourdan, F., Verati, C., Feraud, G., 2006. Intercalibration of the Hb3gr Ar-40/Ar-39 dating standard. Chem Geol 231, 177-189.

Keil, K., Stoffler, D., Love, S.G., Scott, E.R.D., 1997. Constraints on the role of impact heating and melting in asteroids. Meteoritics and Planetary Science 32, 349-363.

Kennedy, T., Jourdan, F., Bevan, A.W.R., Mary Gee, M.A., Frew, A., 2013. Impact history of the HED parent body(ies) clarified by new 40Ar/39Ar analyses of four HED meteorites and one anomalous basaltic achondrite. Geochim Cosmochim Ac 115, 162-182.

Koppers, A.A.P., 2002. ArArCALC - software for Ar-40/Ar-39 age calculations. Comput Geosci-Uk 28, 605-619.

Korochantseva, E.V., Trieloff, M., Lorenz, C.A., Buykin, A.I., Ivanova, M.A., Schwarz, W.H., Hopp, J., Jessberger, E.K., 2007. L-chondrite asteroid breakup tied to Ordovician meteorite shower by multiple isochron Ar-40-Ar-39 dating. Meteorit Planet Sci 42, 113-130.

Langenhorst, F., Deutsch, A., 2012. Shock Metamorphism of Minerals. Elements 8, 31-36.

Lee, J.Y., Marti, K., Severinghaus, J.P., Kawamura, K., Yoo, H.S., Lee, J.B., Kim, J.S., 2006. A redetermination of the isotopic abundances of atmospheric Ar. Geochim Cosmochim Ac 70, 4507-4512.

Levine, J., Renne, P.R., Muller, R.A., 2007. Solar and cosmogenic argon in dated lunar impact spherules. Geochim Cosmochim Ac 71, 1624-1635.

Lister, G.S., Baldwin, S.L., 1996. Modelling the effect of arbitrary P-T-t histories on argon diffusion in minerals using the MacArgon program for the Apple Macintosh. Tectonophysics 253, 83-109.

McBirney, A.R., 1984. Igneous Petrology. Jones and Bartlett Publishers, Boston.

McDougall, I., Harrison, T.M., 1999. Geochronology and thermochronology by the 40Ar/39Ar method. Oxford University Press, Oxford, New York.

McSween, H.Y., Mittlefehldt, D.W., Beck, A.W., Mayne, R.G., McCoy, T.J., 2011. HED Meteorites and Their Relationship to the Geology of Vesta and the Dawn Mission. Space Sci Rev 163, 141-174.

Mittlefehldt, D.W., McCoy, T.J., Goodrich, C.A., Kracher, A., 1998. Non-chondritic meteorites from asteroidal bodies. Reviews in Mineralogy 36, XVII-XVIII.

Nowak, M., Schreen, D., Spickenbom, K., 2004. Argon and CO2 on the race track in silicate melts: A tool for the development of a CO, speciation and diffusion model. Geochim Cosmochim Ac 68, 5127-5138.

Osae, S., Misra, S., Koeberl, C., Sengupta, D., Ghosh, S., 2005. Target rocks, impact glasses, and melt rocks from the Lonar impact crater, India: Petrography and geochemistry. Meteoritics and Planetary Science 40, 1473-1492.

Renne, P.R., Balco, G., Ludwig, K.R., Mundil, R., Min, K., 2011. Response to the comment by W.H. Schwarz et al. on "Joint determination of K-40 decay constants and Ar-40*/K-40 for the Fish Canyon sanidine standard, and improved accuracy for Ar-40/Ar-39 geochronology" by PR Renne et al. (2010). Geochim Cosmochim Ac 75, 5097-5100.

Renne, P.R., Mundil, R., Balco, G., Min, K.W., Ludwig, K.R., 2010. Joint determination of K-40 decay constants and Ar-40*/K-40 for the Fish Canyon sanidine standard, and improved accuracy for Ar-40/Ar-39 geochronology. Geochim Cosmochim Ac 74, 5349-5367.

Russell, C.T., Raymond, C.A., Coradini, A., McSween, H.Y., Zuber, M.T., Nathues, A., De Sanctis, M.C., Jaumann, R., Konopliv, A.S., Preusker, F., Asmar, S.W., Park, R.S., Gaskell, R., Keller, H.U., Mottola, S., Roatsch, T., Scully, J.E.C., Smith, D.E., Tricarico, P., Toplis, M.J., Christensen, U.R., Feldman, W.C., Lawrence, D.J., McCoy, T.J., Prettyman, T.H., Reedy, R.C., Sykes, M.E., Titus, T.N., 2012. Dawn at Vesta: Testing the Protoplanetary Paradigm. Science 336, 684-686.

Schiller, M., Baker, J., Creech, J., Paton, C., Millet, M.A., Irving, A., Bizzarro, M., 2011. Rapid timescales for magma ocean crystallization on the howardite-eucrite-diogenite parent body. Astrophys J Lett 740.

Schmieder, M., Jourdan, F., 2013. The Lappajärvi impact structure (Finland): Age, duration of crater cooling, and implications for early life. Geochim Cosmochim Ac 112, 321-339.

Scott, E.R.D., Greenwood, R.C., Franchi, I.A., Sanders, I.S., 2009. Oxygen isotopic constraints on the origin and parent bodies of eucrites, diogenites, and howardites. Geochim Cosmochim Ac 73, 5835-5853.

Shuster, D.L., Balco, G., Cassata, W.S., Fernandes, V.A., Garrick-Bethell, I., Weiss, B.P., 2010. A record of impacts preserved in the lunar regolith. Earth Planet Sc Lett 290, 155-165.

Spivak-Birndorf, L.J., Bouvier, A., Wadhwa, M., Bland, P.A., Spurný, P., 2010. Trace Element Geochemistry and Chronology of the Bunburra Rockhole Basaltic Achondrite, Lunar and Planetary Institute Science Conference Abstracts, p. 2274.

Spray, J.G., 2010. Frictional melting processes in planetary materials: From hypervelocity impact to earthquakes, pp. 221-254.

Therriault, A.M., Fowler, A.D., Grieve, R.A.F., 2002. The Sudbury Igneous Complex: A Differentiated Impact Melt Sheet. Economic Geology 97, 1521-1540.

Weiss, B.P., Elkins-Tanton, L.T., 2013. Differentiated Planetesimals and the Parent Bodies of Chondrites. Annual Review of Earth and Planetary Sciences 41, 529-560.

Weirich, J.R., Isachsen, C.E., Johnson, J.R., Swindle, T.D. 2012. Variability of diffusion of argon in albite, pyroxene, and olivine in shocked and unshocked samples. Geochimica et Cosmochimica Acta 77, 546–560.

Welten, K.C., Meier, M.M.M., Caffee, M.W., Laubenstein, M., Nishizumi, K., Wieler, R., Bland, P.A., Towner, M.C., Spurny, P., 2012. Cosmic-ray exposure age and preatmospheric size of the Bunburra Rockhole achondrite. Meteorit Planet Sci 47, 186-196.

Wünnemann, K., Collins, G.S., Osinski, G.R., 2008. Numerical modelling of impact melt production in porous rocks. Earth Planet Sc Lett 269, 529-538.

Yamaguchi, A., Clayton, R.N., Mayeda, T.K., Ebihara, M., Oura, Y., Miura, Y.N., Haramura, H., Misawa, K., Kojima, H., Nagao, K., 2002. A new source of basaltic meteorites inferred from Northwest Africa 011. Science 296, 334-336.

Figure Captions

Fig.1: (a) Thin section photograph of the Bunburra basaltic achondrite in polarized light. (b) Scanning electron microscope image of Bunburra. Note the absence of melt and diaplectic glass, and the abundance occurrence of cracks.

Fig.2: $^{40}Ar/^{39}Ar$ age spectra measured for five coarse-grained aliquots (~250 μm in diameter each) of the Bunburra eucrite using laser step heating. Ages have been calculated using the ^{40}K decay constants of Renne et al. (2011) and the R-value$_{(FCs/Hb3gr)}$ of Jourdan and Renne (2007).

Fig. 3: $^{40}Ar/^{39}Ar$ age spectra measured for four fine-grained particles (~250 μm in diameter each) of the Bunburra eucrite.

Fig. 4: Seven individual plateau and mini-plateau ages for coarse- and fine-grains particles from the oldest age population obtained for the Bunburra eucrite particles. Note the absence of correlation between age and grain size. A weighted mean age of 3640 ± 18 Ma (P=0.53) has been calculated from the seven individual ages. Full external error propagation using the optimization model of (Renne et al., 2010) and R-value$_{(FCs/Hb3gr)}$ uncertainty of Jourdan and Renne (2007) yields an external uncertainty of ± [21] Ma.

Fig. 5: Nine individual plateau and mini-plateau ages ranked by increasing age and showing two distinct age populations of ca. 3.64 and 3.54 Ga.

Fig. 6: Low temperature steps from the nine age spectra obtained from the Bunburra eucrite particles (Fig. 2 and 3). These steps represent between 10 and 28% of the total gas of each age spectrum.

Fig. 7: $^{40}Ar/^{39}Ar$ vs. $^{40}Ar/^{36}Ar$ inverse isochron plots of five aliquots extracted from the fusion crust surrounding the Bunburra meteorite that fell on Earth in 2007 (Bland et al., 2009). Four particles show atmospheric composition and zero-age. SG1 show that residual radiogenic $^{40}Ar^*$ is present in the system likely related to the presence of unmelted crystals.

Fig. 8: K/Ca ratio of the fusion crust particles. Four particles show a homogenous K/Ca ratio suggesting that the plagioclase and pyroxene crystals have been fully melted and homogenized in a glass state. SG1 show a variable K/Ca suggesting that discrete crystals did not melt and were trapped in the glass.

Fig. 9: A-T–t diagrams (Jourdan et al., 2010; Jourdan et al., 2007). Solid curves indicate the T-t conditions required to fully reset a sphere of 150 μm radius. Fields located on the right/upper side of the curves indicate complete $^{40}Ar^*$ reset for a given mineral. Red curve= plagioclase; purple curve = basalt, green curve = pyroxene, dashed green curve = leaky pyroxene, dashed blue line = pyroxene (Pb). D_0 and E_a values are given in the text. Dashed gray curves represent A-T-t path of a given sphere immediately after impact. If the A-T-t path crosscut a solid curve, this means that the sphere is age-reset for a given mineral/rock type. A) T-t condition immediately after impact ($1x10^7$ s = 116 days) Solidus temperatures of

plagioclase and basalt are indicated but are not valid for time shorter than a few seconds (Eq 1; Fig. 10). B) Same as (A) but for slow cooling (sub-equilibrium) conditions up to 1 Ma after impact. A-T-t path calculated using a cooling rate of 500°/Ma (Schmieder and Jourdan, 2013). Pb curve in pyroxene is not shown but is approximately constant above 1100°C.

Fig. 10: A-T-t diagram for plagioclase and pyroxene spheres of 150 μm radius. Solid line represents the total Ar reset curves shown in Fig. 9. The dashed line depicts a unique set of possible T-t pair conditions required to remove 15% of the total $^{40}Ar^*$ in the plagioclase sphere, at the time of the event. The gray area represents the conditions where plagioclase is in solid form (Eq 1; Annex 2). For very brief period of time, a higher amount of energy is required to melt the system. The blue dashed line represents the reset curve of Pb in pyroxene.

Fig. 11: Synthetic spectra calculated using the McArgon program (Forster and Lister, 2010; Lister and Baldwin, 1996) for a 150 μm radius eucrite sphere made of 60% plagioclase and 40% pyroxene and for two different T-t histories assuming a formation age at 4.5 Ga and an impact event at 3.64 Ga (dashed line). D_0 and E_a values are given in the text.

Fig. 12: Summary of impact events recorded by the Bunburra eucrite. We interpret these events as follow: event 1 and event 2 are impact-induced melting events on a single melt rock but at two different emplacements. Event 3 is a brecciation event responsible for the amalgamation of the various lithologies observed in the Bunburra achondrite (Fig. 1).

Table 1: Summary of plateau and mini-plateau ages of nine Bunburra basaltic fragments. Plateaus are defined by more than 70% ^{39}Ar released and $P > 0.05$. Mini-plateaus are defined by 50-70% ^{39}Ar released. Event 1 ≈ 3.64 Ga; event 2 ≈ 3.54 Ga. Internal errors do not include

the uncertainties on the ^{40}K decay constants and uncertainties on the age of the Hb3gr standard. MSWD and P-values are indicated. A P-value above 0.05 indicates a concordant series of steps.

Annex 1: Complete Ar isotopic abundances and analytical parameters for each sample (coarse grained, fine grained and fusion crust). Sheet data generated by ArArCALC (Koppers, 2002).

Annex 2: K/Ca step-heating plots for the coarse and fine breccia lithology samples.

Annex 3: Detailed thermodynamic model equations to constrain time-temperature basalt melting conditions upon impact.

Sample N°	Event dated	Plateau age (Ma)	Internal errors (2s)	All sources of errors (2s)	Total ^{39}Ar released (%)	Attribute	MSWD	P
Coarse breccia								
SG-1	1	**3623**	**±53**	**±55**	76%	Pl	0.7	0.71
SG-2	1	*3656*	*±52*	*±53*	53%	Mini-Pl	1.12	0.35
SG-3	2	**3538**	**±30**	**±31**	82%	Pl	0.69	0.83
SG-4	1	**3647**	**±34**	**±35**	90%	Pl	0.84	0.65
SG-5	2	*3553*	*±38*	*±39*	51%	Mini-Pl	1.57	0.09
Fine groundmass								
SG-1	1	**3622**	**±60**	**±62**	85%	Pl	0.64	0.72
SG-2	1	**3612**	**±107**	**±108**	81%	Pl	1.82	0.09
SG-3	1	**3596**	**±56**	**±57**	88%	Pl	0.65	0.77
SG-4	1	*3658*	*±35*	*±36*	63%	Mini-Pl	0.95	0.68
				Table 1: Jourdan et al.				

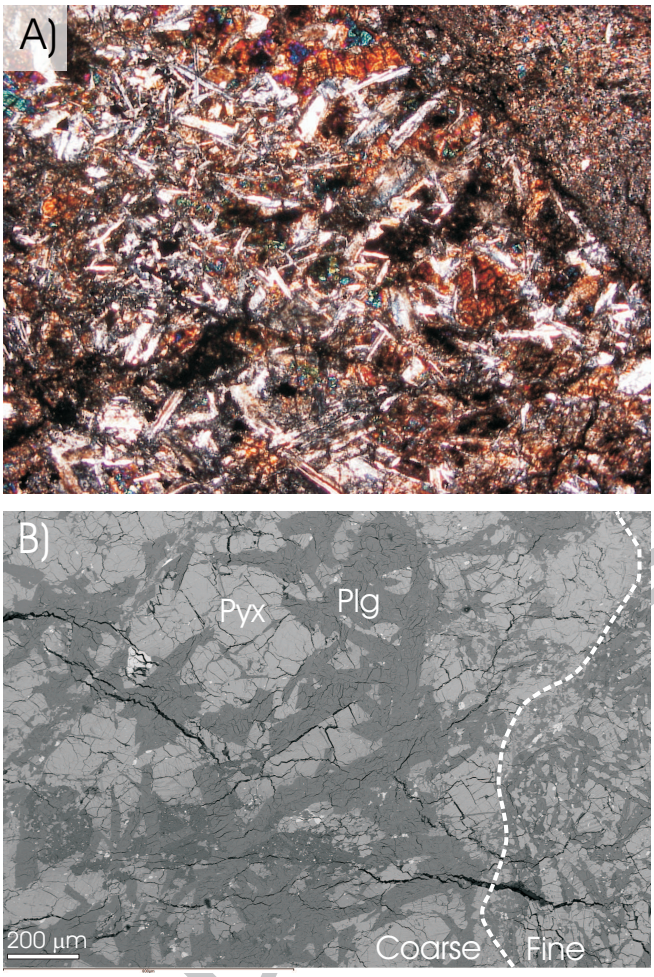

Fig. 1: Bunburra meteorite: Jourdan et al.

Fig. 2 - Plateaus_coarsegrained.pdf

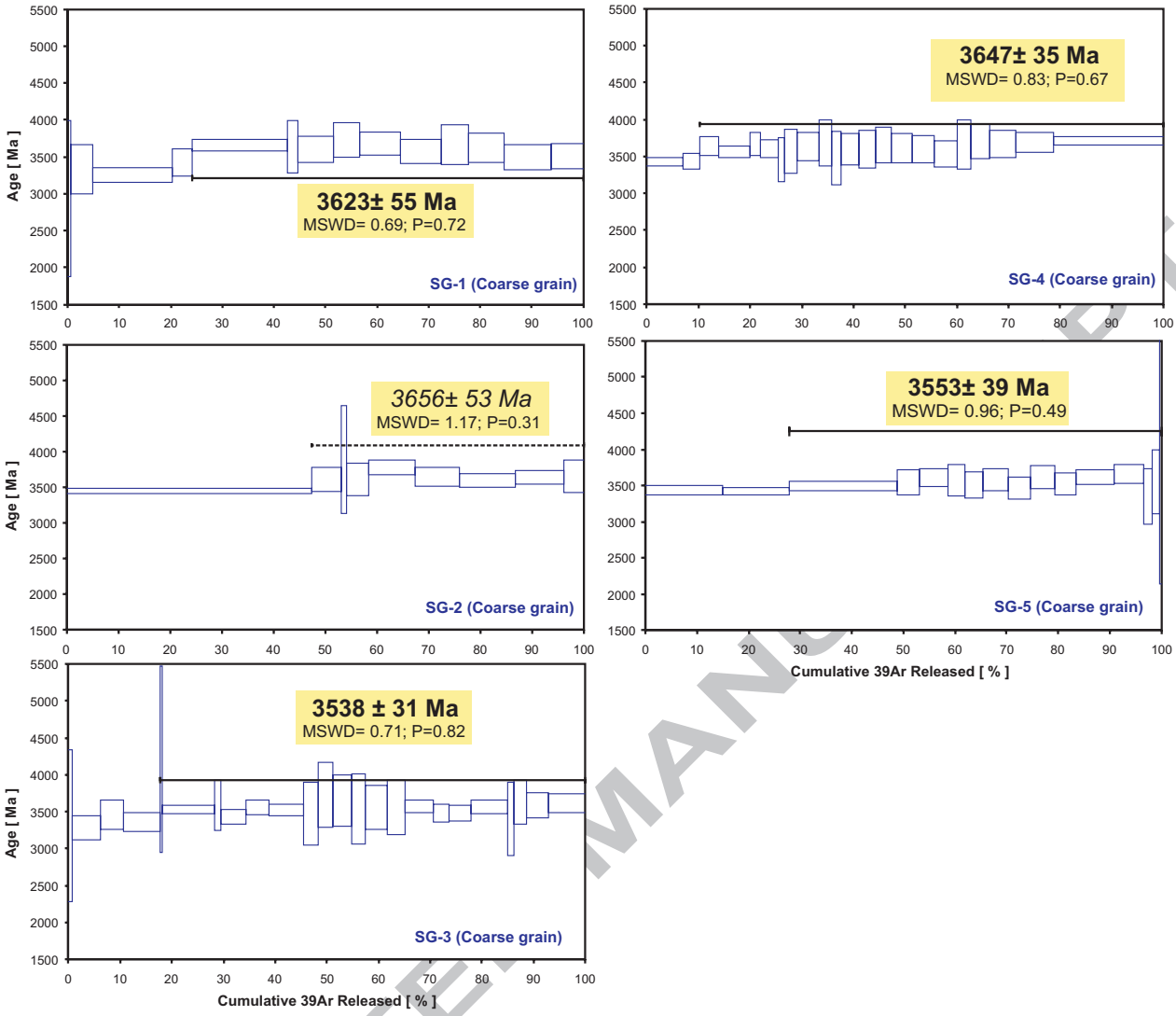

Fig.2 Plateaus_coarse: Jourdan et al.

Fig. 3 - Plateaus_finegrained.pdf

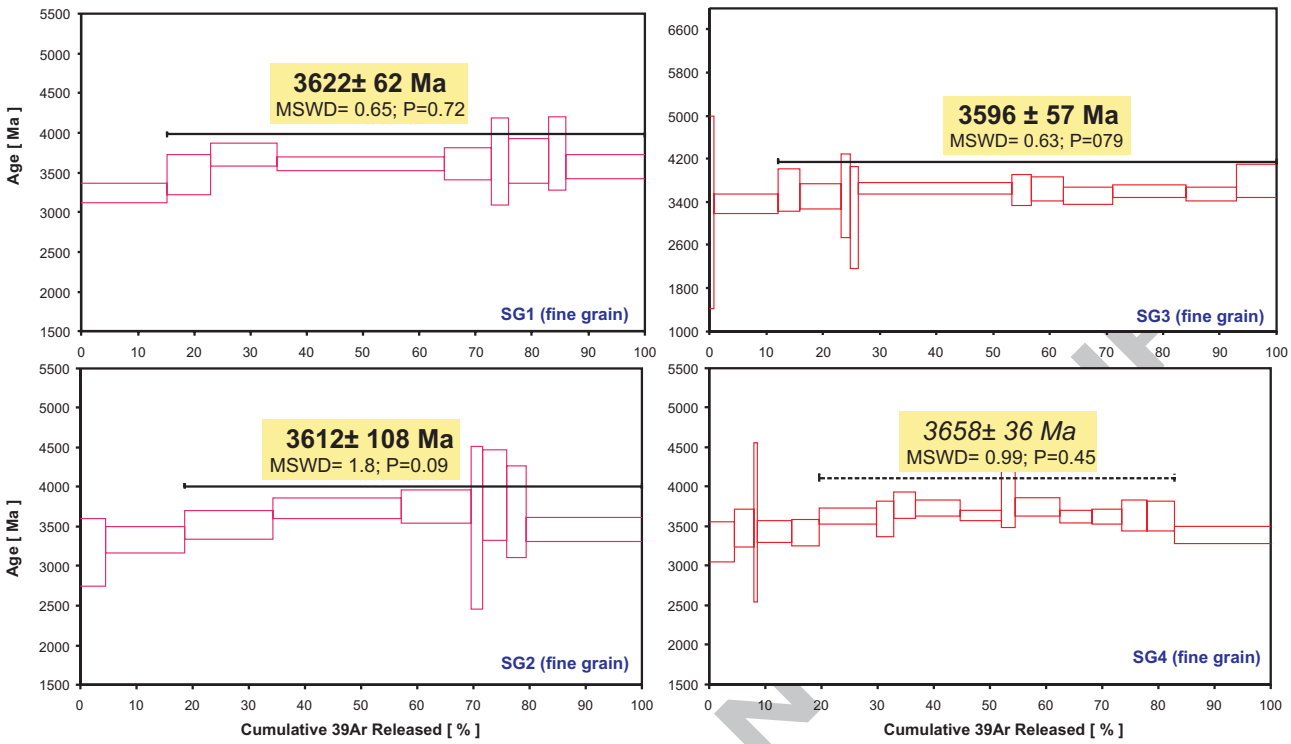

Fig.3 Plateaus_fine: Jourdan et al.

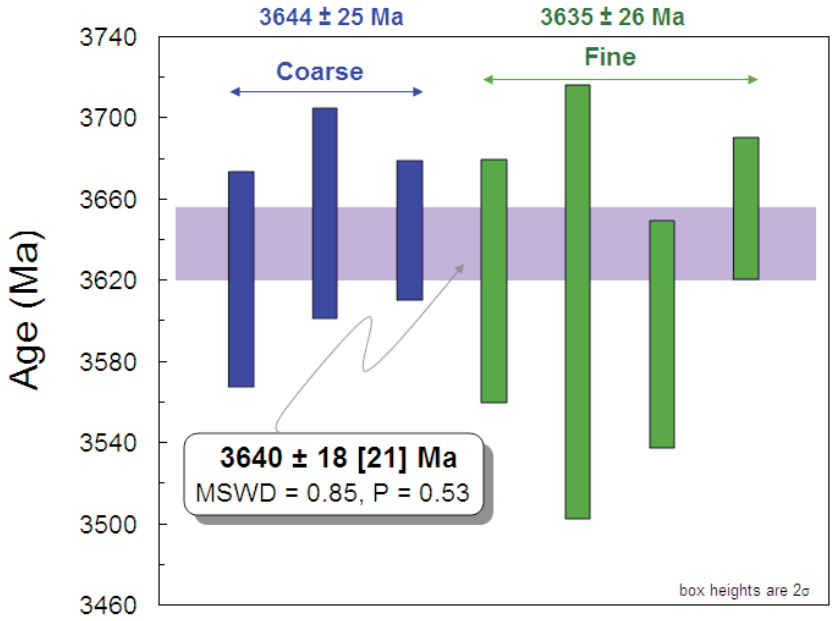

Fig. 4_age Bunburra: Jourdan et al.

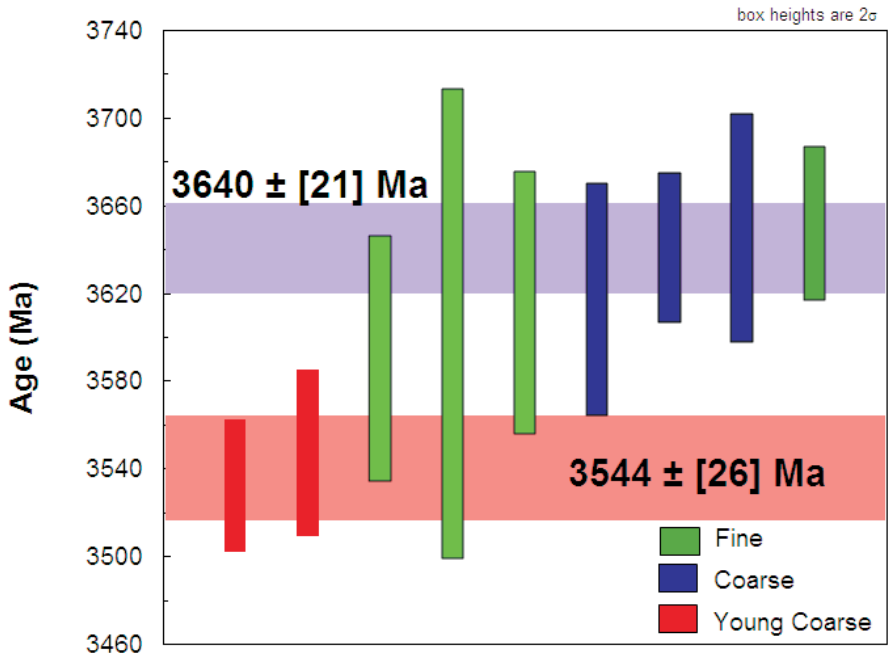

Fig.5_age 2 events: Jourdan et al.

Fig. 6 - low temp steps

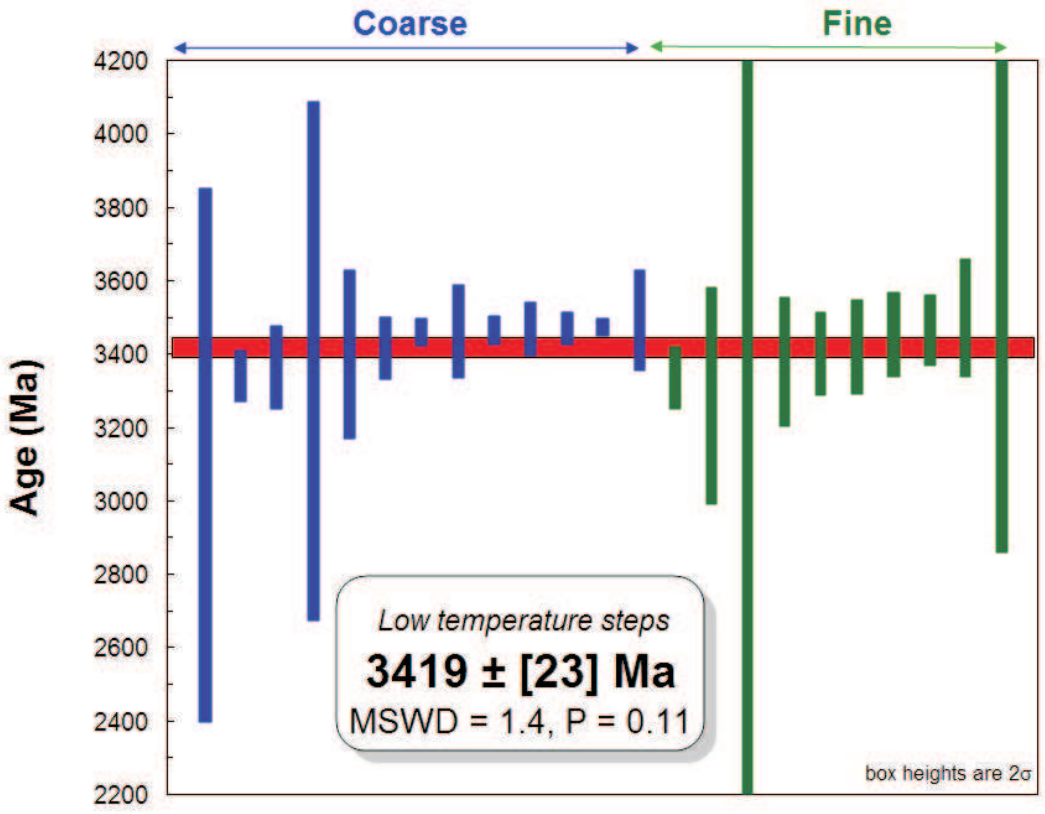

Fig. 6_lowT steps: Jourdan et al.

Fig. 7 - Isochron Fcrust.pdf

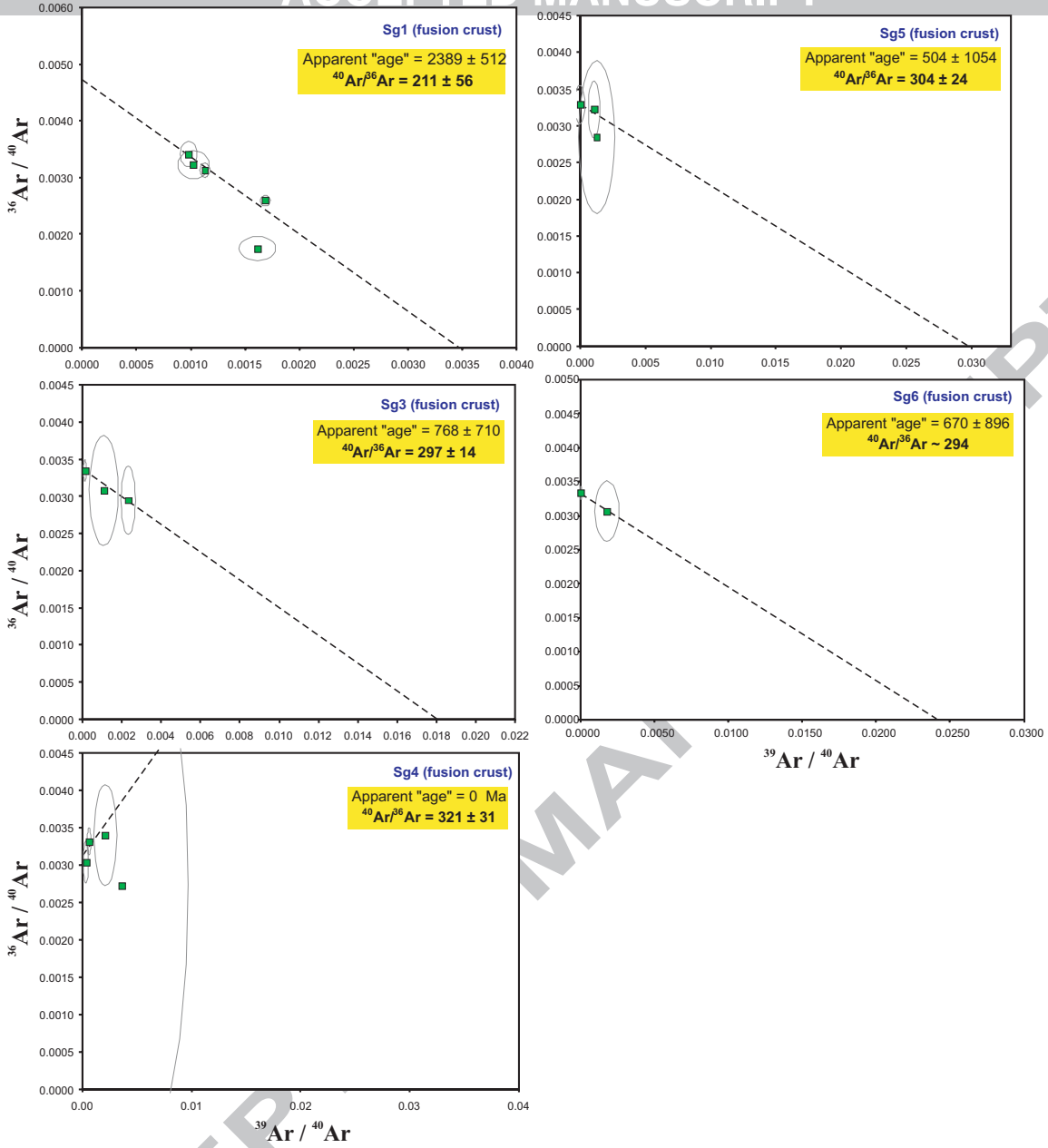

Fig. 7 - isochron Fusion crust

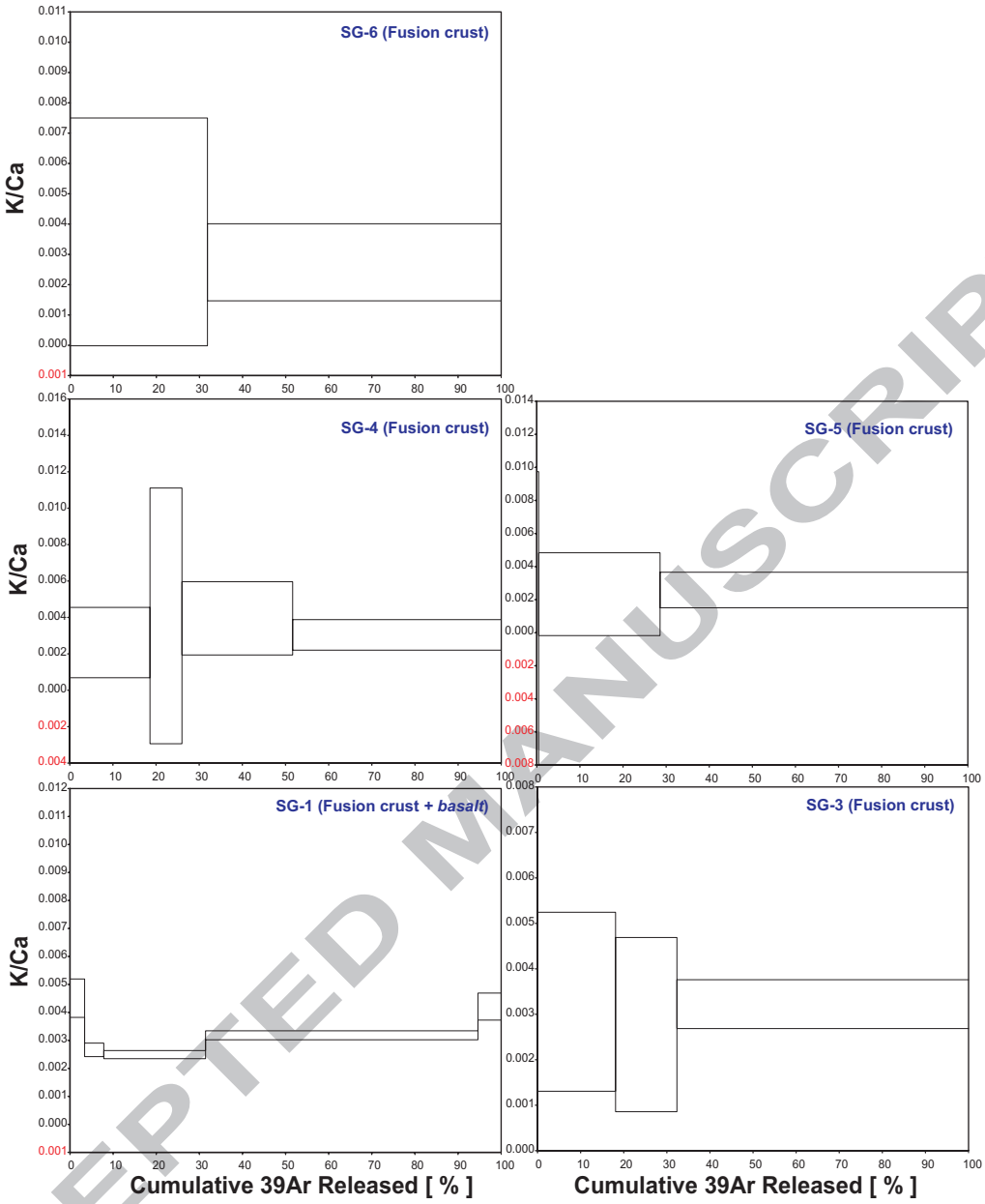

Fig. 8 - Ca/K Fcrust: Jourdan et al.

Figure 9 - Ar reset curves

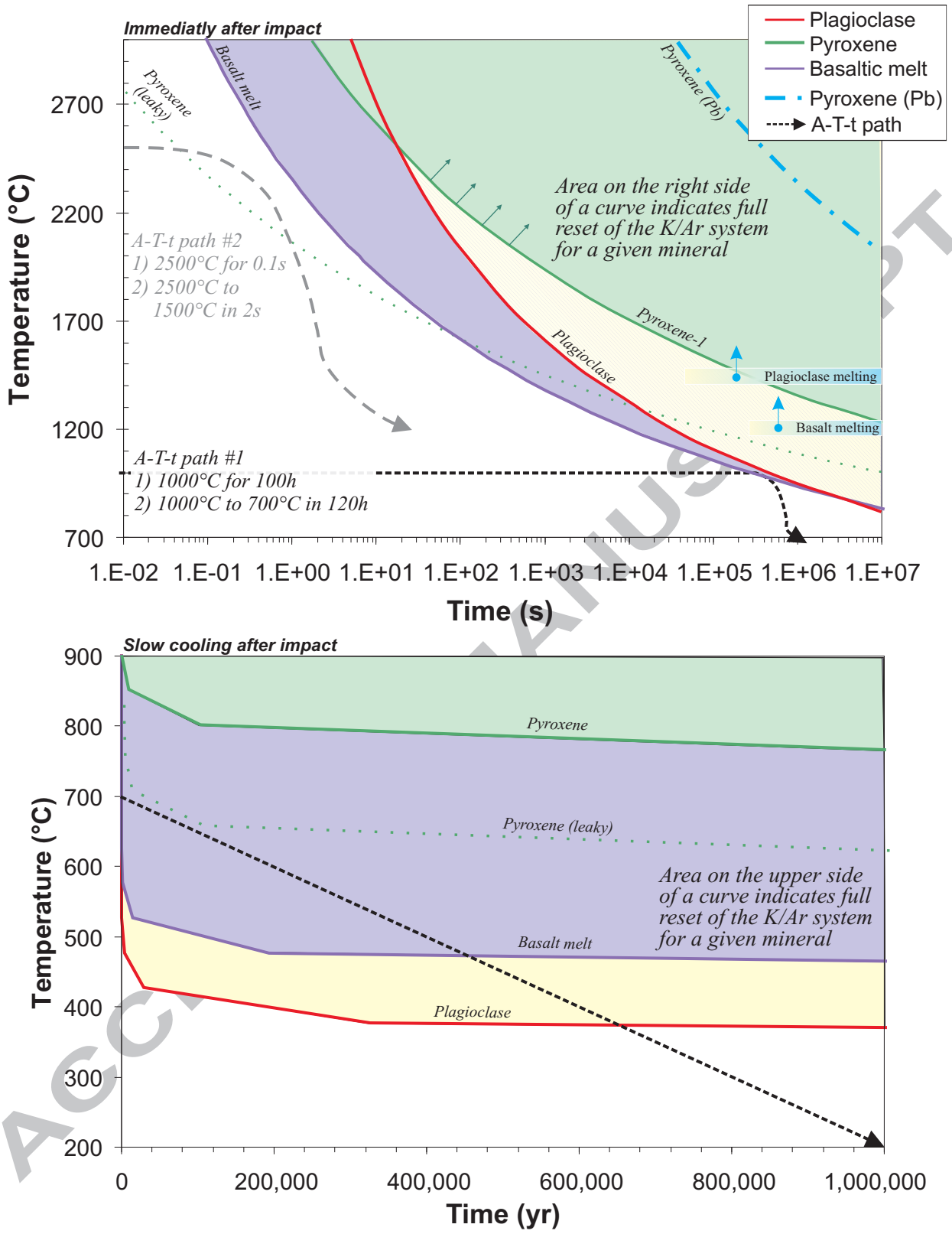

Fig. 9 - A-T-t curves: Jourdan et al.:

Figure 10 - Curve15%loss

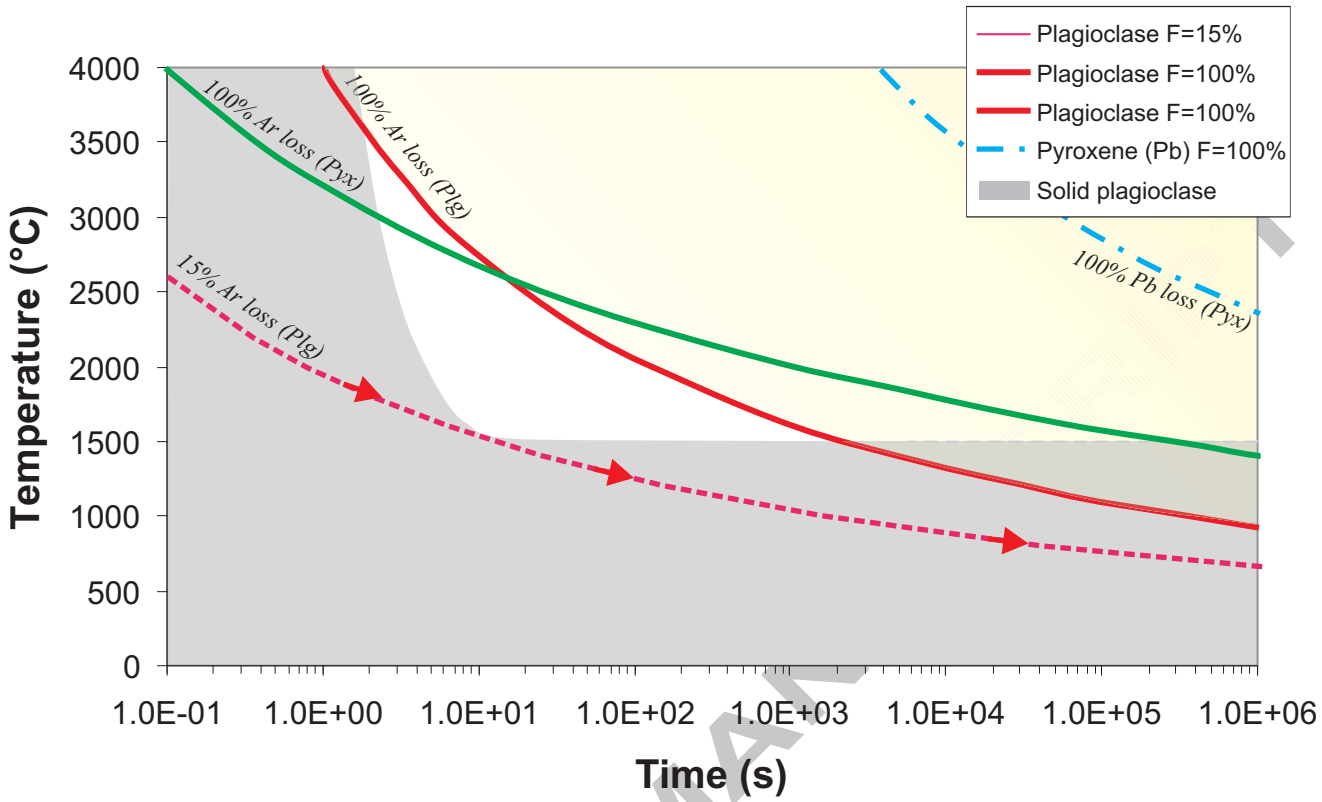

Fig.10 - 15%Arloss: Jourdan et al.

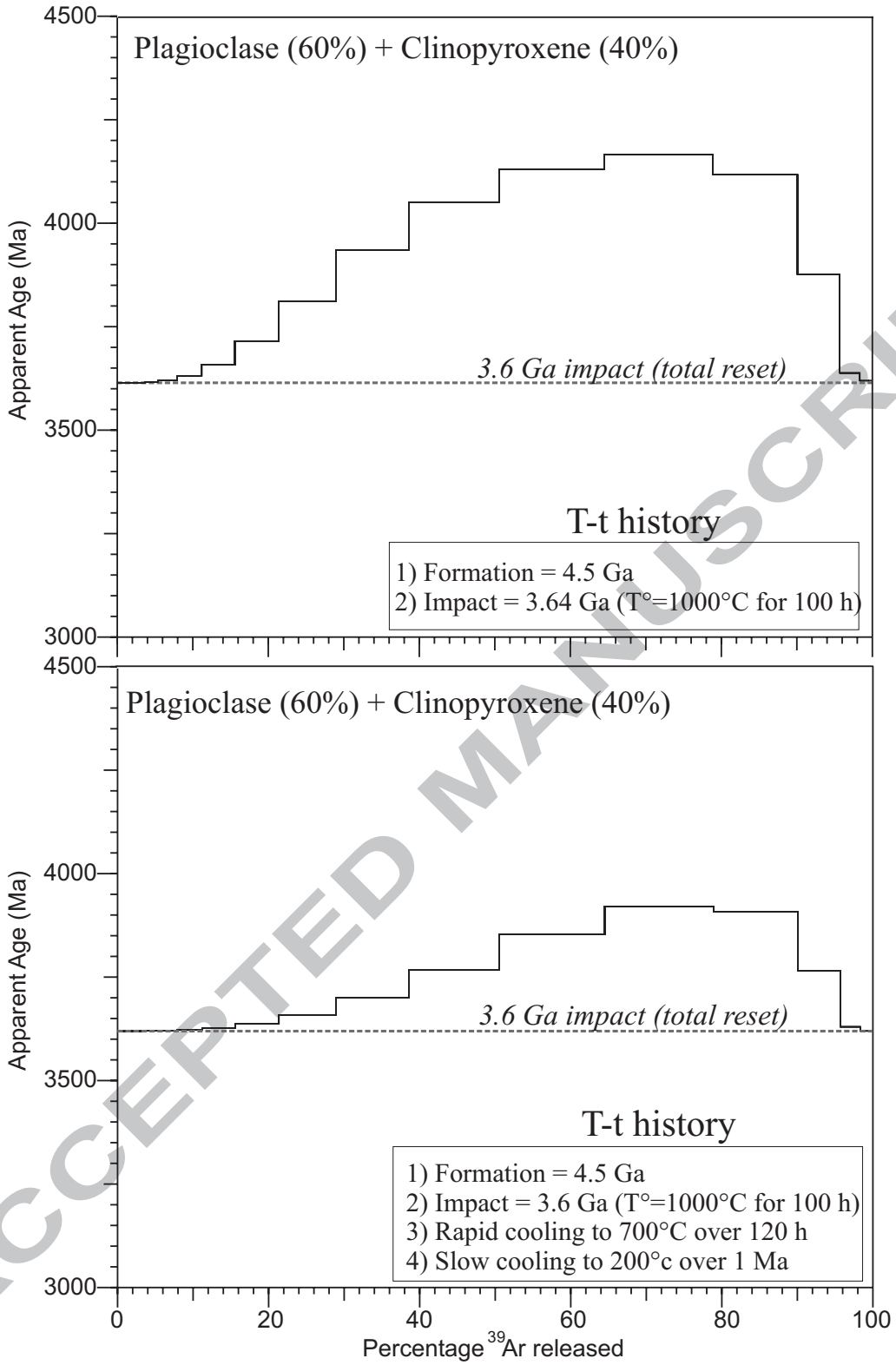

Fig. 11 - synthetic spectra: Jourdan et al.

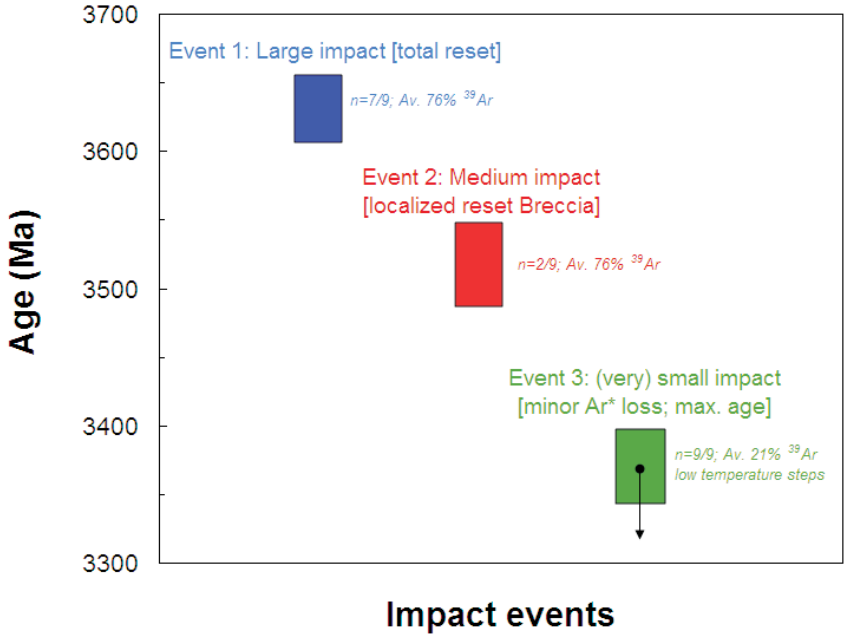

Fig. 12 Events summary: Jourdan et al.